NTNU – Trondheim
Norwegian University of
Science and Technology

Lowering and lifting operations through moonpools: Hydrodynamic investigations

Sigve Håland

Marine Technology
Submission date: June 2014
Supervisor: Marilena Greco, IMT

Norwegian University of Science and Technology
Department of Marine Technology

Lowering and lifting operations through moonpools: Hydrodynamic investigations

Stud. Techn. Sigve Håland

June 13, 2014

Scope of work

Moonpools are used in many types of vessels to launch and recover equipment, divers or diving bells, or lay cables or risers, or sub-sea modules, so to protect them from the waves. One must however guarantee that this system is suitable to this scope. This is not true, for example, if the column of water enters in resonant condition, excited by the waves and the heave motion of the vessel. In the latter case, the oscillations of the fluid inside the moonpool can have amplitudes several times larger than the heave motion of the vessel. The project thesis examined the moonpool system through a literature study and focused on the analysis of available experiments on a specific module being lowered through moonpool on a given installation vessel and tried to reproduce the measured vertical force acting on the module using DNV recommended practice.

Objective

The aim of the thesis is to continue and deepen the investigations performed during the project; to examine occurrence of resonance phenomena inside moonpools used in practical applications; to further assess DNV recommended practice and to examine the applicability of existing numerical methods for the simulation of this type of operations. The focus of the thesis is on hydrodynamic aspects.

The work should be carried out in steps as follows:

1. Summarize major findings/outcomes from the project thesis and extend the literature study in terms of resonance (piston and sloshing) phenomena in moonpools and of possible suppression devices adopted.
2. Study existing experiments in terms of launching techniques, i.e. over the side of the vessel, through a standard moonpool and through an enlarged moonpool, and in terms of other relevant features for a chosen heading condition. Compare trends and safety and challenges for the different techniques.
3. Select a numerical strategy to investigate this type of operations, justify your choice and describe its parts and the related solution algorithm to

perform the time-domain simulations of the lowering. Apply the numerical strategy to reproduce results from model tests, also comparing against results from DNV recommended practice.

4. Using the selected numerical approach carry on a systematic comparative investigation of a standard and an enlarged moonpool from hydrodynamic point of view. From these and previous studies in item 2, discuss advantaged and challenges in using different sized moonpools.

5. Discuss how the available knowledge of moonpools can be used to make the analysis part simplified in the early stages of design.

The work may show to be more extensive than anticipated. Some topics may therefore be left out after discussion with the supervisor without any negative influence on the grading.

The candidate should in his report give a personal contribution to the solution of the problem formulated in this text. All assumptions and conclusions must be supported by mathematical models and/or references to physical effects in a logical manner.

The candidate should apply all available sources to find relevant literature and information on the actual problem.

The thesis should be organised in a rational manner to give a clear presentation of the work in terms of exposition of results, assessments, and conclusions. It is important that the text is well written and that tables and figures are used to support the verbal presentation. The thesis should be complete, but still as short as possible. In particular, the text should be brief and to the point, with a clear language. Telegraphic language should be avoided.

The thesis must contain the following elements: the text defining the scope (i.e. this text), preface (outlining project-work steps and acknowledgements), abstract (providing the summary), table of contents, main body of thesis, conclusions with recommendations for further work, list of symbols and acronyms, references and (optional) appendices. All figures, tables and equations shall be numerated.

The supervisor may require that the candidate, in an early stage of the work, present a written plan for the completion of the work. The plan should include budget for the use of computer and laboratory resources that will be charged to the department. Overruns shall be reported to the supervisor.

From the thesis it should be possible to identify the work carried out by the candidate and what has been found in the available literature. It is important to give references to the original source for theories and experimental results.

The thesis shall be submitted in two copies:

- The copies must be signed by the candidate.
- This text, defining the scope, must be included.
- The report must appear in a bound volume or a binder.
- Drawings and/or computer prints that cannot be included in the main volume should be organised in a separate folder.
- The bound volume shall be accompanied by a CD or DVD containing the written thesis in World or PDF format. In case computer programs have been made as part of the thesis work, the source codes shall be included. In case of experimental work, the experimental results shall be included in a suitable electronic format.

Supervisor: Marilena Greco

Submitted: 16. January 2014

Deadline: 10. June 2014

Marilena Greco
Supervisor

Preface

This report is the master thesis conducted by Stud. Techn. Sigve Håland for the Department of Marine Technology. The work was preformed during the final semester of the master program.

The purpose of the thesis is to study the hydrodynamic effects that occur inside a moonpool. The results of model tests performed by Technip and numerical simulations of the problem have been used to gain insight to the topic.

The intention of this thesis was to run time domain simulations in OrcaFlex. Due to problems with the panel model in WAMIT, the work was delayed and time domain simulations were not performed. The frequency domain results from WAMIT are used in stead.

I would like to thank my supervisor Prof. Marilena Greco for good help and guidance during my work on the thesis. Peng Li has also been very helpful by sharing his knowledge about how to properly use WAMIT.

This thesis has been written in cooperation with Technip Norge AS. They have provided all the relevant data and made all their recourses available for this work. In addition they have given valuable inputs to the thesis.

Trondheim, June 13, 2014

Sigve Håland

Abstract

On construction vessels subsea modules, diving bells, cables and so on are often lifted through a moonpool. The advantage of using a moonpool is that the surface elevation inside the moonpool is shielded against the outside waves. Further, the moonpool is often located close to the vessels center of rotation, which makes the lifting operation less sensitive to vertical motions due to roll and pitch. For some frequencies the water inside the moonpool may be excited in a resonant condition such as sloshing or so-called piston mode. In these cases the benefit of using a moonpool may be outweighed by the large resonant excitation. This thesis compares the hydrodynamic properties between a regular sized moonpool and a moonpool that is significantly larger.

First, the results from a model test campaign for a specific offshore operation have been analyzed. The campaign was performed in irregular waves with a construction vessel moored in a stationary position with modules inside the moonpool. The results are indicating that modules are shielded from the incident waves, especially for the high frequent waves where the response is almost cancelled. There are some indications for a resonant piston mode occurring, but with a very low amplification. The largest amplifications are close to 1. Meaning that the wave height inside the moonpool is similar to the wave height of the incident wave.

Finally, the vessel has been modeled and analyzed numerically using the potential theory based panel method. The software WAMIT has been used to calculate responses due to radiation and diffraction. The surface elevation indicates that the piston mode is very large for the standard size moonpool compared to the enlarged moonpool. However, when the moonpool is enlarged, a sloshing mode becomes more dominant.

Comparing the experimental and the numerical method has proven to be challenging. The model test was performed for a very complex system with a lot of details that are hard to replicate; both from a modeling point of view and with regards to all the physical effects that should be accounted for.

Samandrag

Påkonstruksjonsskip vert ofte undersjøiske modular, dykkeklokker, kablar og såvidare løfta gjennom moonpool. Fordelen med ånytte moonpool er at vassflata inni moonpool er skjerma fråbølgjene som kjem utanfrå. I tillegg er moonpool ofte plassert i nærleiken av rotasjonssenteret påskipet. Dette gjer løfteoperasjonen mindre var for dei vertikale rørslene som kjem av rulle- og stamperørslene til skipet. For nokre frekvensar kan vassflata bli eksitert i resonante tilstandar som stempel-mode eller såkalla skvalpe-mode. I desse høva kan den store resonante eksitasjone vege tyngre enn fordelane med ånytte moonpool. Denne avhandlinga samanliknar dei hydrodynamiske eigenskapane til eit moonpool av vanleg storleik med eit mykje større moonpool.

Til åbyrje med blei resultata fråei modelltestkampanje for ein offshore operasjon analyserte. Modelltestinga blei utført i irregulære bølgjer med eit konstruksjonsskip fortøyd i ein stasjonær posisjon med ulike modular i moonpool. Resultata syner at modulane er godt skjerma fråbølgjene utanfrå, spesielt dei mest høgfrekvente som er nesten kansellerte! Ein finn indikasjonar påstempel-moda, men med låg forsterking. Dei største forsterkingane er om lag 1. Det vil seie at bølgjehøgda inni moonpool er om lag like høg som den innkomande bølgja.

Til slutt har skipet blitt modellert og analysert numerisk med panelmetoden som bygg påpotensialteori. Programvaren WAMIT har rekna ut responsen som kjem frådiffraksjon og radiasjon. Vassflatehevinga syner at stempelmoda er veldig stor for stempel-moda i det vanlege moonpoolet samanlikna med det store moonpoolet. Påden andre sida, er ei skvalpe-mode meir dominerande for det store moonpoolet.

Det har vist seg åvera utfordrande åsamanlikna den eksperimentelle og den numeriske metoden. Modelltesten vart utført for eit veldig komplekst system med mange detaljar som er vanskelege åetterlikne. Dette både med tanke påmodellering og dei fysiske effektane ein bør rekne med.

Contents

List of Figures

Nomenclature

A	Moonpool cross section area $[m^2]$
A_m	Projected area of the module $[m^2]$
C_A	Added mass coefficient $[-]$
C_D	Drag coefficient $[-]$
C_{A0}	Added mass coefficient for unrestricted flow $[-]$
C_{D0}	Drag coefficient for unrestricted flow $[-]$
D	Vessel draft $[m]$
F_N	Froudes number $[-]$
H_S	Significant wave height $[m]$
H_{m0}	Significant wave height based on the zeroth spectral moment $[m]$
T_p	Spectral peak period $[s]$
κ	Moonpool cross section parameter $[-]$
f	Spectral frequency $[1/s]$
t	time $[s]$
ρ_m	Density of fresh water $[kg/m^3]$
ρ_s	Density of sea water $[kg/m^3]$

Introduction

Subsea gas compression is a key to boost the recovery of certain offshore gas fields. Statoil has decided to put a subsea gas compression unit on the seabed next to the Midgard gas field to transport the gas to the existing Åsgard field. The reservoir pressure in Midgard is too low for the gas to be transported by itself. Without the compression unit, the reserves in Midgard would have been left untouched. The project is the first of its kind worldwide and the unit is known to become the world's largest subsea machine. Technip has been awarded the job of installing the subsea unit with all the modules. The template was installed during the summer 2013 and the modules will be installed into the template the following two or three seasons.

Lowering modules through moonpools is often a preferred method as it is less sensitive to weather conditions. Technip considers to lower most of the modules through the moonpool of the OSV North Sea Giant(NSG). One of the worlds most sophisticated offshore construction vessels. The structure of the OSV NSG is designed so that the existing moonpool can be enlarged. The analysis of the possible lifting operation is very complicated because of the complexity of the structure and the size of the moonpool. Therefore, model testing has been performed to obtain more knowledge about the operation.

In this thesis the hydrodynamic properties of a standard size moonpool with dimensions $7.2m * 7.2m$ will be compared with an enlarged moonpool with dimensions $16m * 16m$

Chapter 1

Theory

According to Molin [2001], a moonpool is a "vertical opening through the deck and hull of ships or barges, used for marine and offshore operations, such as pipe laying or recovery of divers." Gaillarde and Cotteleer [2004] says that operations inside the moonpool are to some point protected against the ocean waves and vessel motions. This is however not the case if the water enters the moonpool in a resonant condition, excited by the waves and the heave motion of the ship. This condition is often referred to in the literature as piston mode. Internal sloshing can also occur in a resonant condition.

Gaillarde and Cotteleer [2004] divides occurrence of moonpool resonant oscillations into two distinct situations: In calm water with forward speed and in waves in a stationary condition. These phenomena are illustrated in Figure 1.1. Of course a combination of the two situations can also provide oscillations. In this paper, only the case without forward speed will be studied. That is because the studied marine operation will be executed with DP station keeping without forward speed.

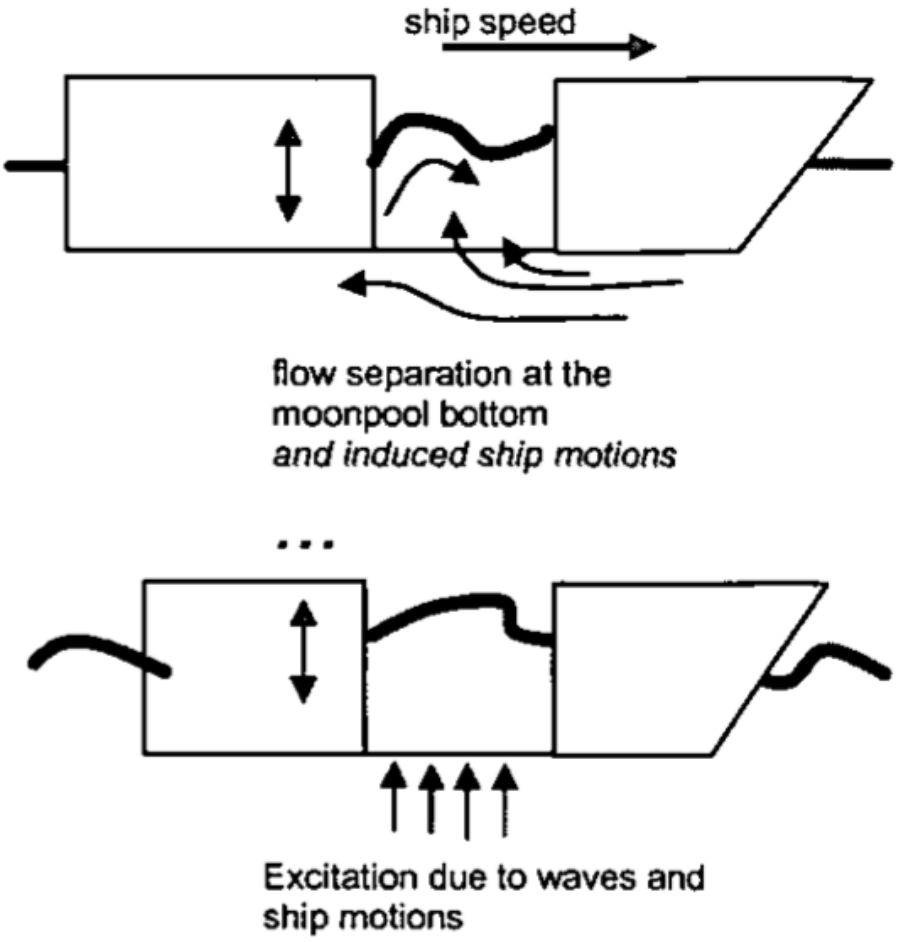

Figure 1.1: Excitation mechanisms inside a moonpool

1.1 Previous studies

There is a lot of studies available on the various phenomena that occur inside the moonpool. Molin [2001] has studied, by applying linear potential theory, the eigenvalue problem inside moonpools. Simplified analytical methods were applied to estimate the resonant periods and shapes for the piston mode and sloshing modes. The results are primarily given with respect to ratios of beam, draft and moonpool size. The studies were performed two-dimensional and three-dimensional.

Further, Faltinsen et al. [2007] performed similar studies, but in a more exact manner and restricted to 2D. They also considered amplitudes and phase shifts. In addition they performed experimental analysis of a catamaran like structure consisting of two rectangular ship hulls to confirm the analytical

approach.

Kristiansen [2009] studied the piston mode that occurs between an LNG carrier and an offshore LNG terminal. Here more applicable methods have been performed to define the piston "body" motion. Even though this is not a moonpool study, the results from this thesis can be applied.

1.2 Piston and sloshing modes

The piston mode and the sloshing modes are known to be the most crucial resonant responses that occur inside moonpools. The water inside the moonpool is modeled as a trapped body that oscillates vertically. This is known at the piston mode. The sloshing modes, however, can be regarded as standing waves inside the moonpool. The shapes of these modes are illustrated in Figure 1.2

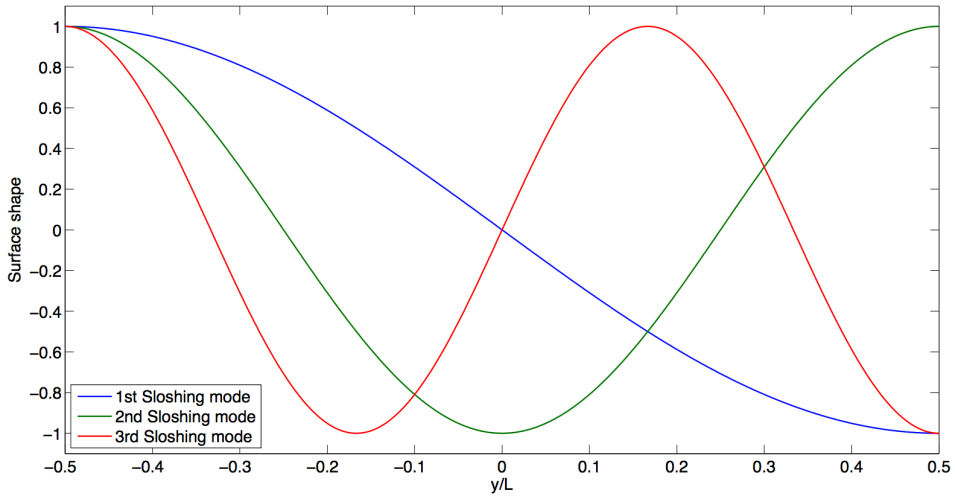

Figure 1.2: Idealized surface shape of the first three sloshing modes

Molin [2001] studied the two-dimensional moonpool problem assuming a long barge with draught h, beam B and moonpool width b. In order to mimic the free surface outside the vessel, a pair of sinks were located outside the hull at locations $y = \pm\lambda B/2 = \pm H/2$. Where λ is a factor somewhat larger than one. According to Kimmoun and Molin [2000], a value of $\lambda \cong 1.5$ gives reasonable results.

Based on Molin [2001], the natural period for the two dimensional piston mode can be obtained as:

$$\omega_0 \cong \sqrt{\frac{g}{h + (b/\pi)(3/2 + ln(H/2b))}} \tag{1.1}$$

and for the first three sloshing modes it can be obtained as:

$$\omega_1 \cong g\frac{\pi}{b}coth(\frac{\pi h}{b} + 1.030) \tag{1.2}$$

$$\omega_2 \cong 2g\frac{\pi}{b}coth(\frac{2\pi h}{b} + 1.488) \tag{1.3}$$

$$\omega_3 \cong 3g\frac{\pi}{b}coth(\frac{3\pi h}{b} + 1.666) \tag{1.4}$$

Using these formulas and $T = 2\pi/\omega$, the natural period sensitivity for the moonpool width is illustrated in Figure 1.3.

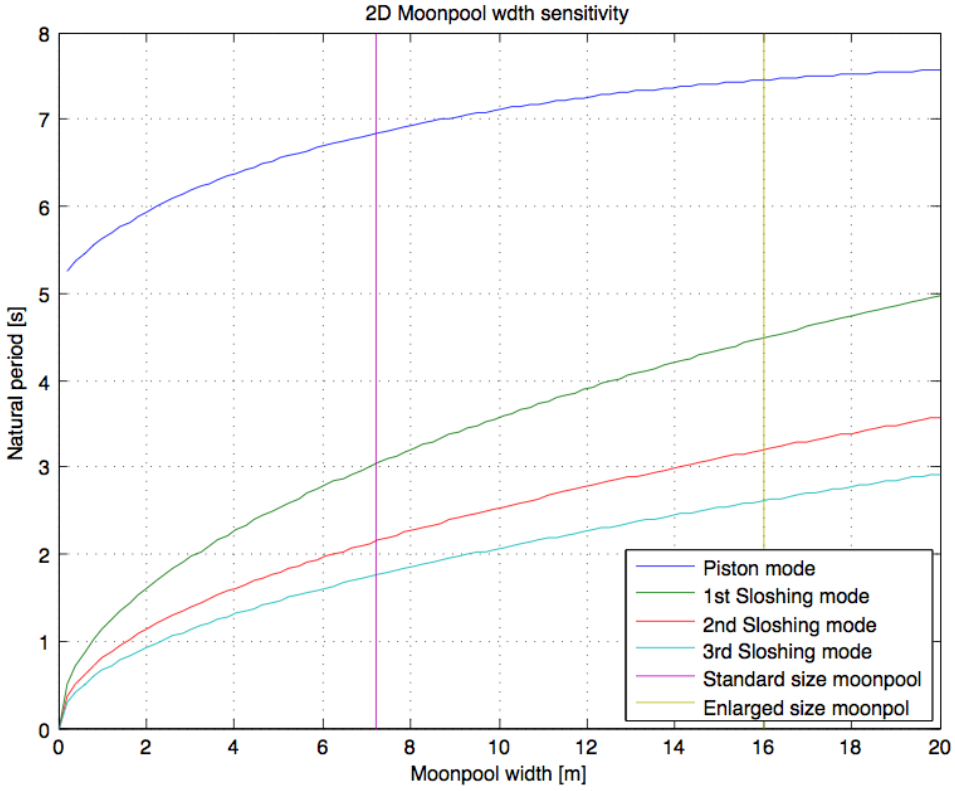

Figure 1.3: Sensitivity of natural periods due to moonpool width

1.3 Flow separation

The bilge vortices formed by the LNG-carrier in waves, were studied by Kristiansen [2009]. It is reasonable to assume that these results can be adapted to moonpool problems. The piston mode inside moonpools is similar to the piston mode that may occur between the LNG-carrier and the terminal. The vortex shedding around the corner of the moonpool inlet is assumed to have a significant non-linear contribution to the damping of the oscillating water plug in piston mode.

In order to investigate this, Kristiansen [2009] set up a numerical wave tank based on non linear potential theory. The basic idea of this tank is illustrated in Figure 1.4. To account for the damping contribution, an inviscid vortex tracking model was included.

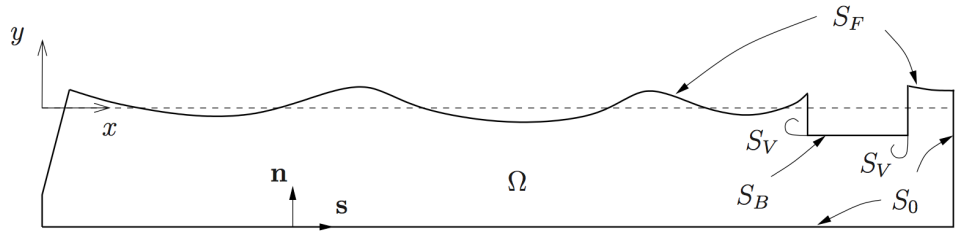

Figure 1.4: Tank considered for numerical experiments by Kristiansen [2009]

Figure 1.5 illustrates the basic principle behind flow separation in the wake a sharp corner. There will be a boundary layer of finite thickness δ that will increase away from the separation point due to diffusion. This shear layer thickness is however assumed to be infinitely thin ($\delta \to 0$) in the inviscid vortex-tracking model.

The results from this model are shown in Figure 1.6. We can observe that as the water is oscillating past the inlet corner, vortices are formed. The first sub-figures (a-h) roughly describe the first oscillating period. Observing the similarities between sub-figure l and n, and between sub-figure m and o, it is reasonable to assume that a steady-state condition is obtained.

Kristiansen [2009] also performed model testing to confirm his model. The results from one of the set ups are presented in Figure 1.7. The upper set of results is for the surface elevation inside the moonpool, while the lower set is for a far away location. We can observe from the graph that the numerical results that accounts for wake, correlates well with the experimental results. Therefore it is reasonable to assume that the vortex shedding gives a major contribution to the damping of the surface elevation.

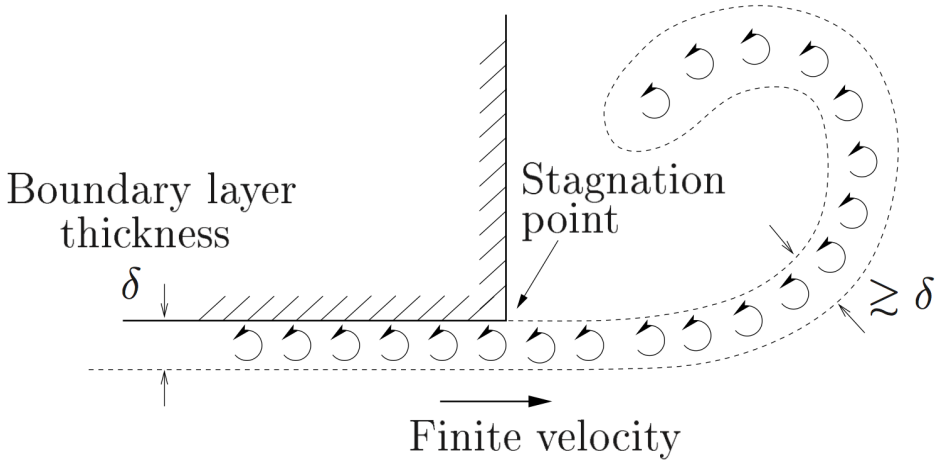

Figure 1.5: Principal sketch of flow separation around corners

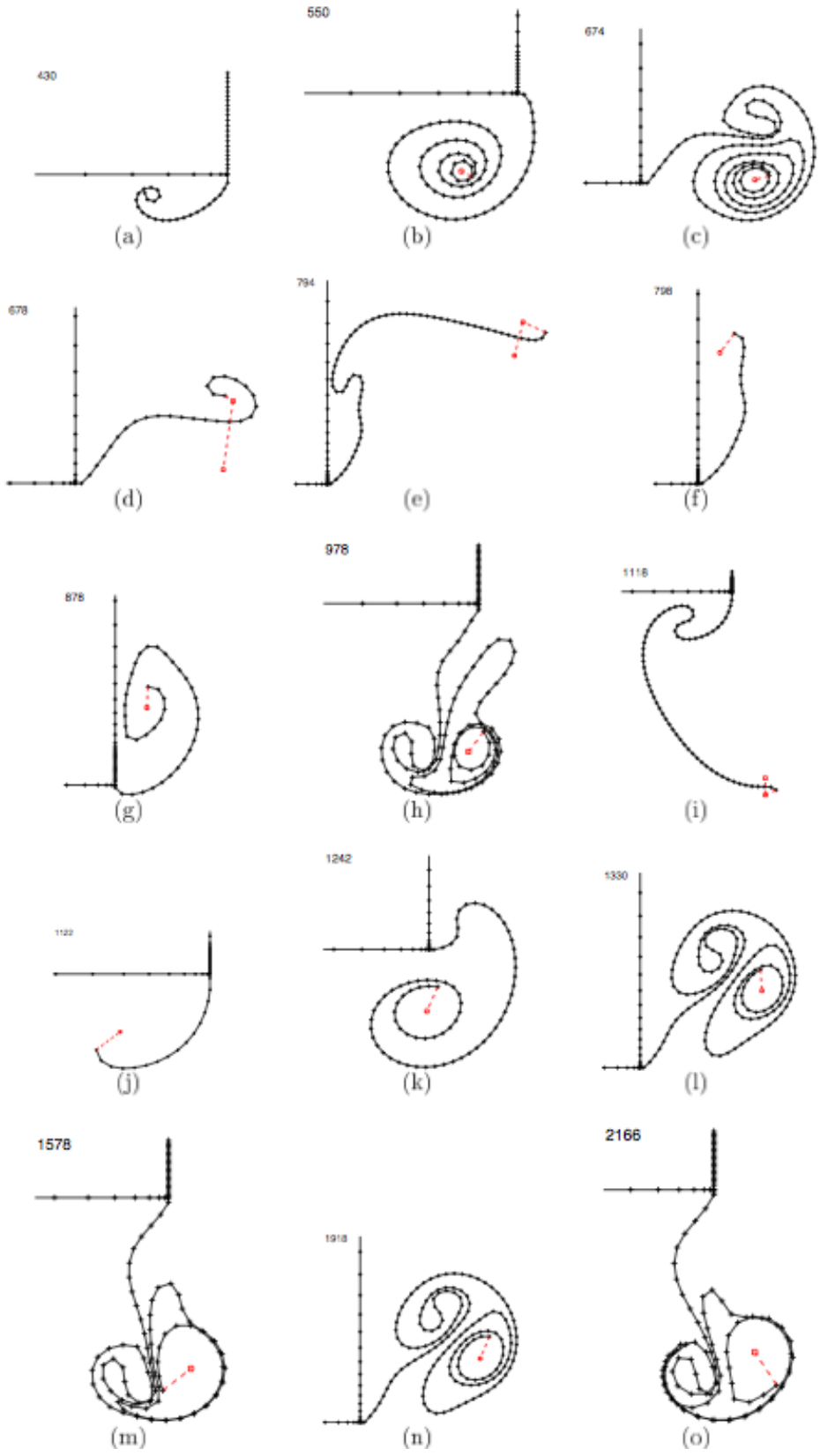

Figure 1.6: Typical initial behavior of the free shear layer Kristiansen [2009]

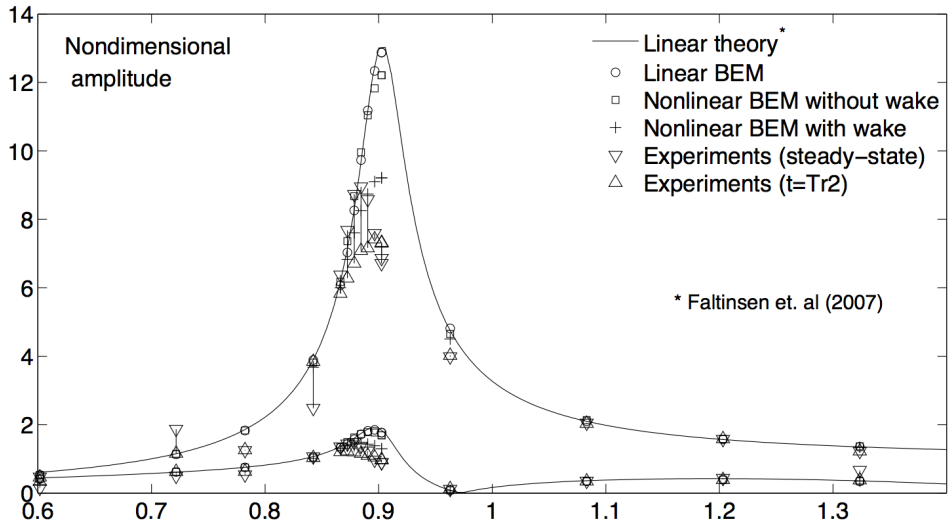

Figure 1.7: Combined numerical and experimental results Kristiansen [2009]

1.4 Suppression Devices

For all practical applications, it is desired to minimize the flow inside the moonpool. That is in resonant condition achieved by maximizing the damping. Since the vortex separation is such a major source of damping, the moonpools should be designed to induce vortices. Sharp corners are more likely to induce vortices than round corners. Therefore, bottom mounted plates as illustrated in Figure 1.8 should induce more distinct vortices and hence increase the damping. This is based on the same principle as the way bilge keels increase the damping for vessels in roll motion. (Faltinsen and Sortland [1987]).

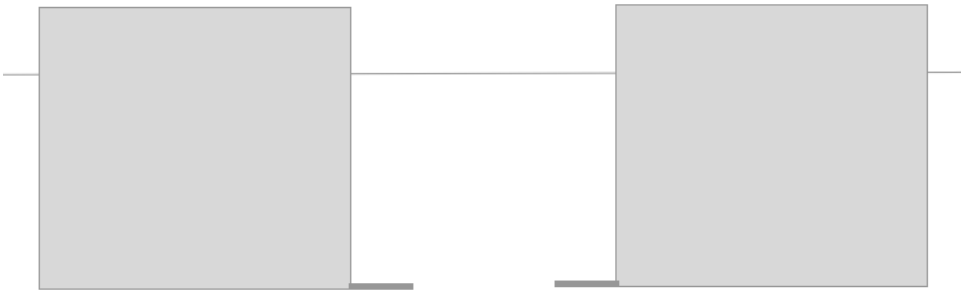

Figure 1.8: Damping plates installed at moonpool bottom

A practical disadvantage of installing the damping plates at the bottom of the moonpool is that they decrease the size of the moonpool opening and limits the size of the modules that can be lowered through the moonpool. The volume above the plates can be fitted with other obstacles such as guidance structures that interrupt the flow. It is common to install perforated walls inside the moonpools as illustrated in Figure 1.9

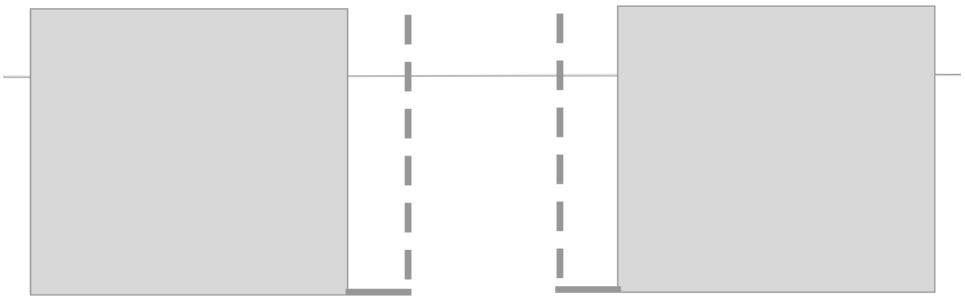

Figure 1.9: Moonpool fitted with perforated walls

In some moonpools, especially moonpools for diving bells, aeration is used to decrease the loads on the bell. During aeration, air is blown into the

moonpool from nozzles close to the bottom of the moonpool. The mix of air and water inside the moonpool will have a lower density than just water. Therefore the hydrodynamic loads on the module should be reduced.

1.5 DNV Recommended Practice

1.5.1 Assumptions

Section 3.5 in DNV [2011] is a simplified analysis method for lifting operations through moonpool. The assumptions for the simplifications are as follows:

1. The moonpool dimensions are small compared to the breadth of the ship.
2. Only motion of water and object in vertical direction is considered.
3. The blocking effect of the lifted object on the water is moderate
4. Cursors prevent impact into the moonpool walls. Only vertical forces parallel to the moonpool axis are considered.

1.5.2 Estimation of resonance period

The resonance period is estimated by using Equation 1.5

$$T_0 = \frac{2\pi}{\sqrt{\frac{K}{A_{33}+M}}} = 2\pi\sqrt{\frac{\rho A(D+\kappa\sqrt{A})}{\rho g A}} = \frac{2\pi}{\sqrt{g}}\sqrt{D+\kappa\sqrt{A}} \tag{1.5}$$

Where κ is a shape parameter for the added mass that is set to $\kappa = 0.46$ for rectangular moonpools.

1.5.3 Force estimation

In order to estimate the applied vertical force on the module, it should first be performed as if the modules were lowered in the open water. The added mass and drag coefficients should be multiplied with an amplification factor. This factor is used since the hydrodynamic forces are increased while the flow around the modules is restricted. The increased drag coefficient and added mass coefficient are given as:

$$\frac{C_D}{C_{D0}} = \frac{1 - 0.5\frac{A_m}{A}}{(1 - \frac{A_m}{A})^2} \tag{1.6}$$

$$\frac{C_A}{C_{A0}} = 1 + 1.9(\frac{A_m}{A})^{\frac{9}{4}} \tag{1.7}$$

Where A_m is the projected area of the module, C_{D0} is the drag coefficient for unrestricted flow and C_{A0} is the added mass coefficient for unrestricted flow.

1.5.4 Damping

As described in section 1.4, the damping of the surface elevation motions is increased when the moonpool is fitted by various suppression devices. This effect is described in Figure 1.10.

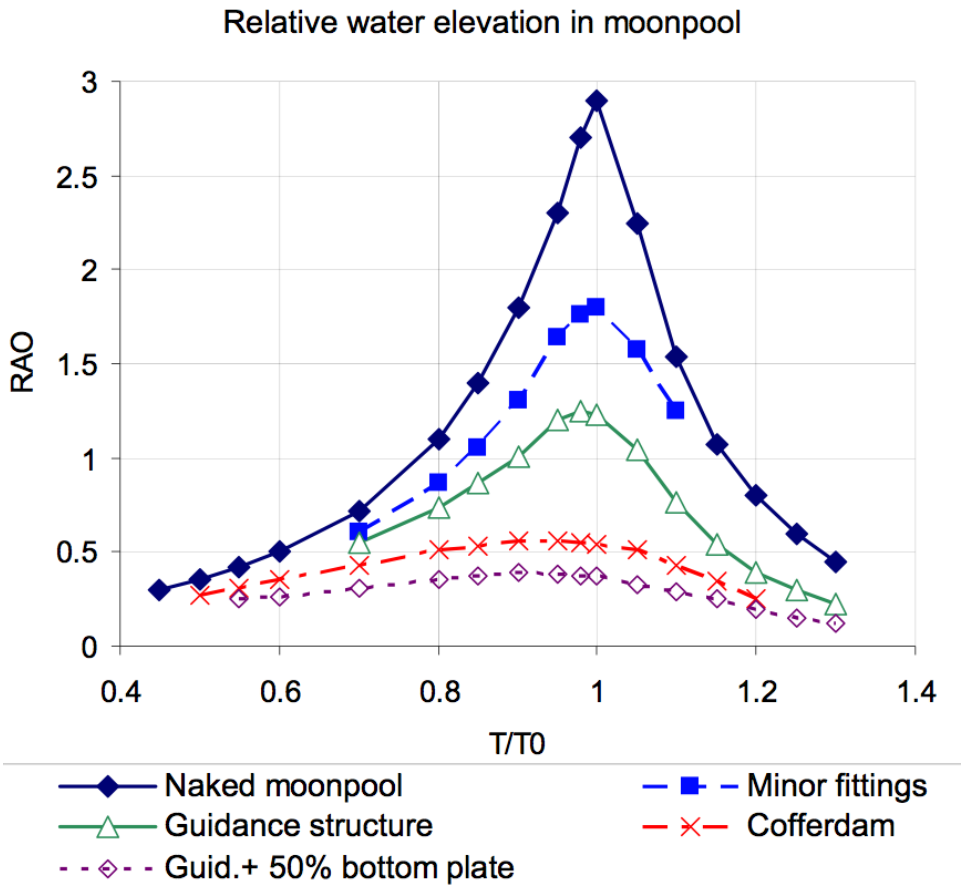

Figure 1.10: Surface elevation RAO for different suppression devices

Chapter 2

Model testing

Oceanide was contracted by Technip Norge AS to perform model testing on structures lowered through the moonpool of OSV North Sea Giant. All the tests were performed in the offshore basin BGO FIRST at La Seyne Sur Mer, France. The purpose of the model testing was to investigate wave loads on Åsgard subsea compression modules during the installation phase. The ship model was moored by a spring system and exposed to irregular waves during the model testing campaign.

All the necessary information about the model test is found in the report provided by Oceanide [2013].

2.1 Scale

The scale factor is set to be $\lambda = 30$. Froude similarity (Equation 2.1) is applied for scaling purposes. This will according to Steen and Minsaas [2012] give similarity in gravitational effects between model scale and full scale. The relevant scaling is given in equations 2.2 through 2.4. The testing facility is using fresh water in the basin. Therefore it is necessary to account for the density difference between sea water and fresh water as seen in Equation 2.4.

$$F_{Ns} = F_{Nm} \tag{2.1}$$

$$Time_s = Time_m * \sqrt{\lambda} \tag{2.2}$$

$$Length_s = Length_m * \lambda \tag{2.3}$$

$$Forces_s = Forces_m * \lambda^3 * \frac{\rho_s}{\rho_m} \tag{2.4}$$

All the data provided by Oceanide [2013] are scaled up to full scale. All the data presented in this thesis will also be in full scale, unless otherwise stated.

2.2 The models

2.2.1 Vessel model

The ship model of the OCV North Sea Giant(Figure 2.1) was fabricated by Oceanide. They built it in polyester glass fiber, and used lead masses to ensure correct displacement, COG and radii of inertia. The vessel is fitted with two different moonpools. One standard size moonpool with cross-section $7.2m * 7.2m$, and one enlarged size moonpool with cross-section $16m * 16m$. The moonpools were built with perforated walls as shown in Figure 2.2. This is to increase the friction and hence the damping of the water motions inside the moonpool as mentioned in section 1.4 in the theory chapter.

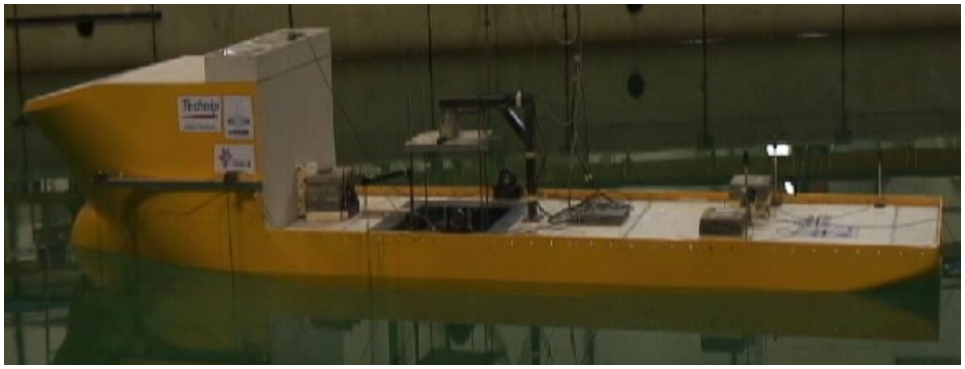

Figure 2.1: Model of OSV North Sea Giant

2.2.2 Module models

The subsea modules that are analyzed in this thesis are the inlet-cooler module, the compressor module and the pump module. The models are simplified and built by Oceanide. The simplification was performed by eliminating small details and applying conservative substitutions as shown in Figure 2.4, Figure 2.5 and Figure 2.6. The pump module was lowered through the standard size moonpool while the compressor module and the inlet-cooler module was lowered through the enlarged size moonpool. The inlet-cooler

During fabrication In place

Figure 2.2: Model of the enlarged size moonpool

During fabrication In place

Figure 2.3: Model of the standard size moonpool

module was also lowered over the side of the vessel in order to compare the two methods of moonpool lowering and over-the-side lowering.

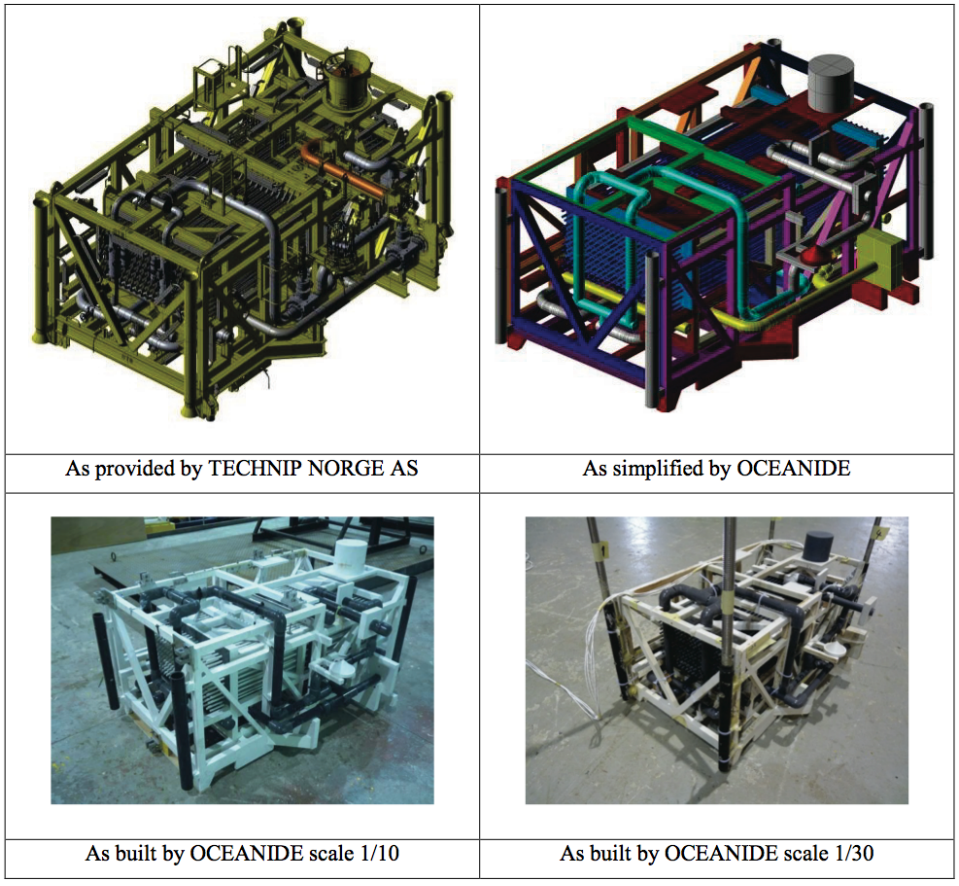

Figure 2.4: Model of the inlet-cooled module

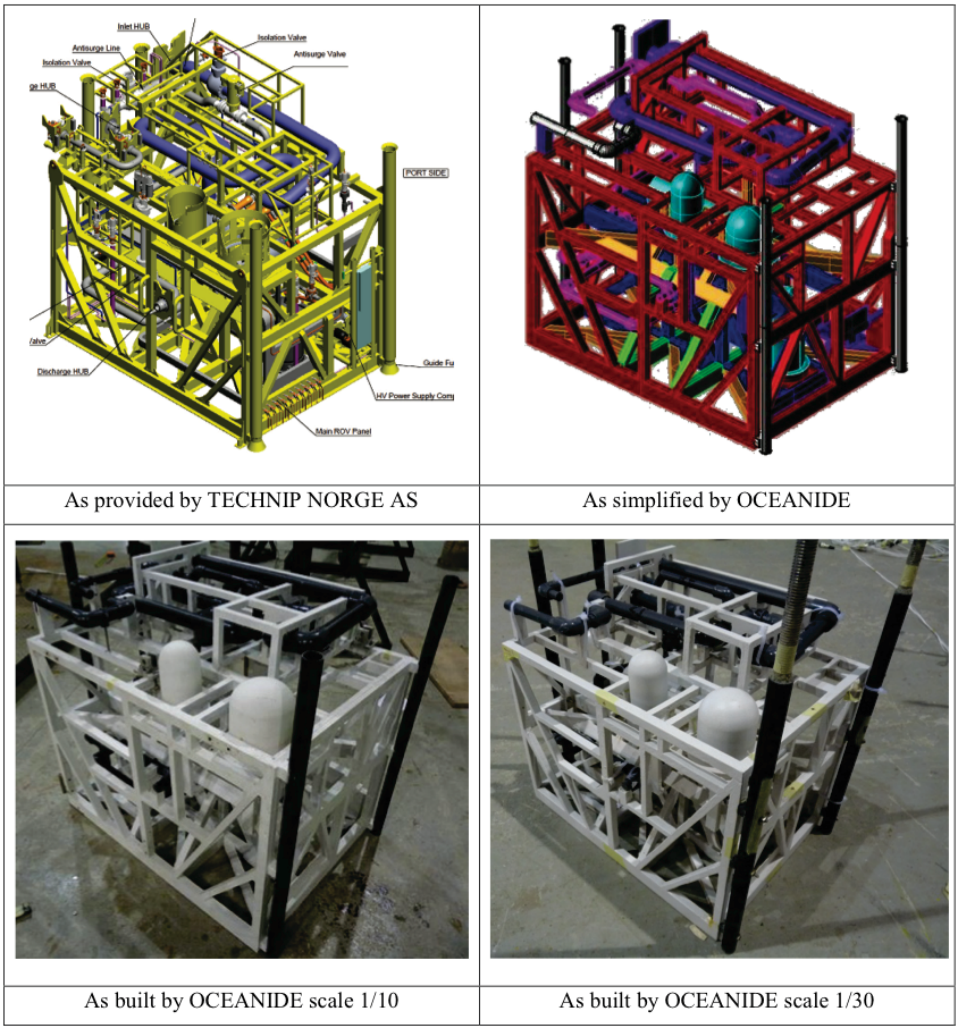

As provided by TECHNIP NORGE AS | As simplified by OCEANIDE

As built by OCEANIDE scale 1/10 | As built by OCEANIDE scale 1/30

Figure 2.5: Model of the compressor module

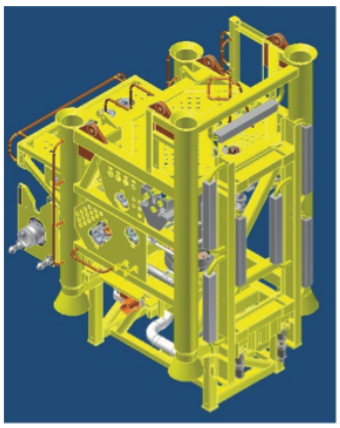

As provided by TECHNIP NORGE AS

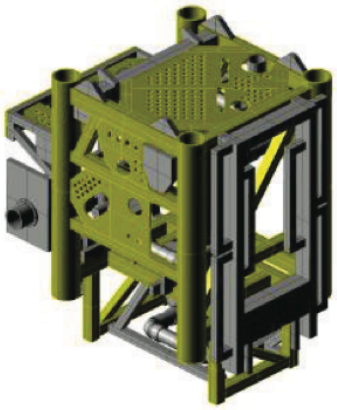

As simplified by OCEANIDE

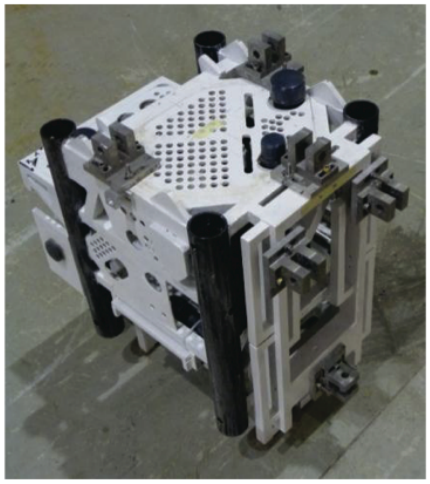

As built by OCEANIDE scale 1/10

As built by OCEANIDE scale 1/30

Figure 2.6: Model of the compressor module

2.3 Test setup

The ship model is moored as shown in Figure 2.7. The mooring was a system of four springs attached at the intersections of the water line and the transverse centerline. This was to prevent the mooring from disturbing the roll motion of the ship model. The vessel was oriented so that the waves will hit the bow of the ship model at an angle of 15° towards the port side.

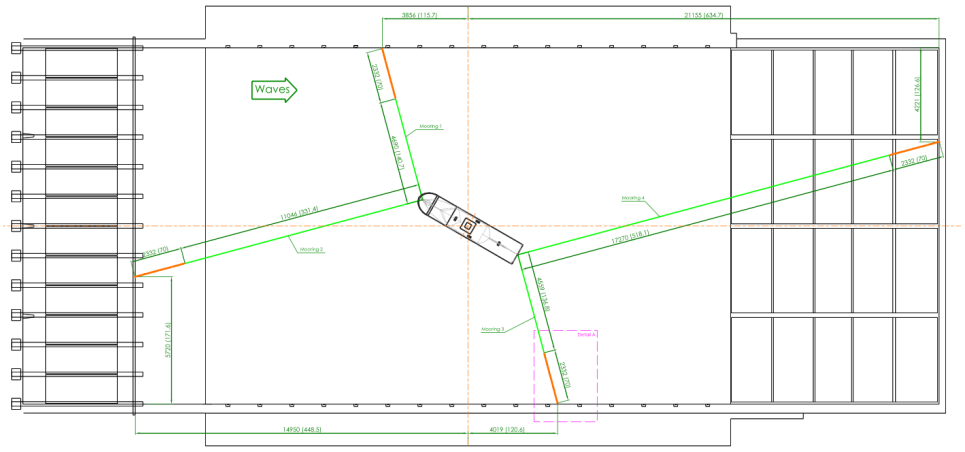

Figure 2.7: Mooring of model

In order to find the different effects in the moonpool throughout the splash zone, the modules were fixed at different elevations as shown in Figure 2.8 through Figure 2.11.

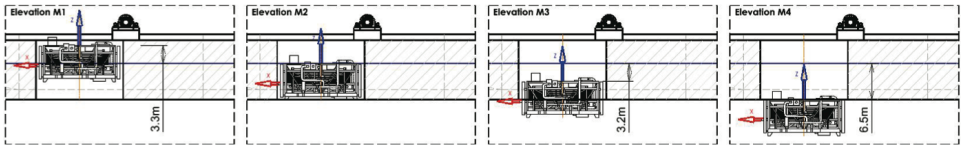

Figure 2.8: Elevations of the inlet-cooler module

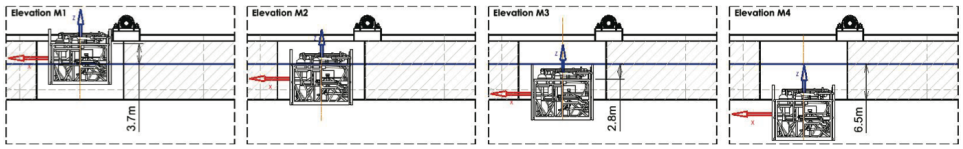

Figure 2.9: Elevations of the compressor module

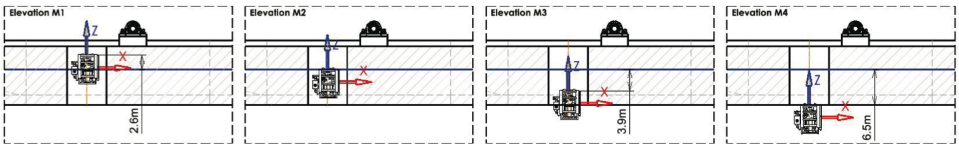

Figure 2.10: Elevations of the inlet-cooler module

Figure 2.11: Elevations of the inlet-cooler module

2.4 Sensors

2.4.1 Motions

The motions of the vessel are measured by the KRYPTON RODYM DMM system. It is a contactless tracking system that uses infrared cameras aiming at markers attached to the model. All six degrees of freedom are found by using the theoretical center of gravity as the origin.

2.4.2 Forces

The forces acting on the modules are found by a six degrees of freedom transducer. As seen in Figure 2.12, the transducer is located so that all forces acting on the module will propagate up the rigid frame system and correctly measured.

2.4.3 Surface elevation

Wave probes measure the surface elevation. They are located alongside the vessel model and one inside the moonpool. The locations of the wave probes are illustrated in Figure 2.13 and Figure 2.14

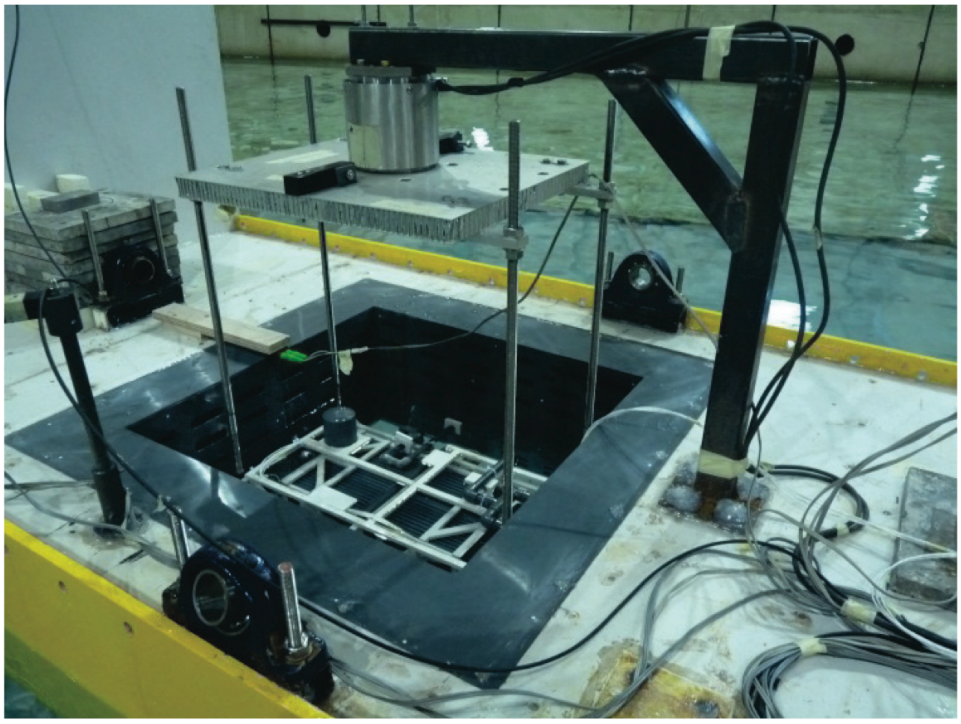

Figure 2.12: Module attached to the transducer

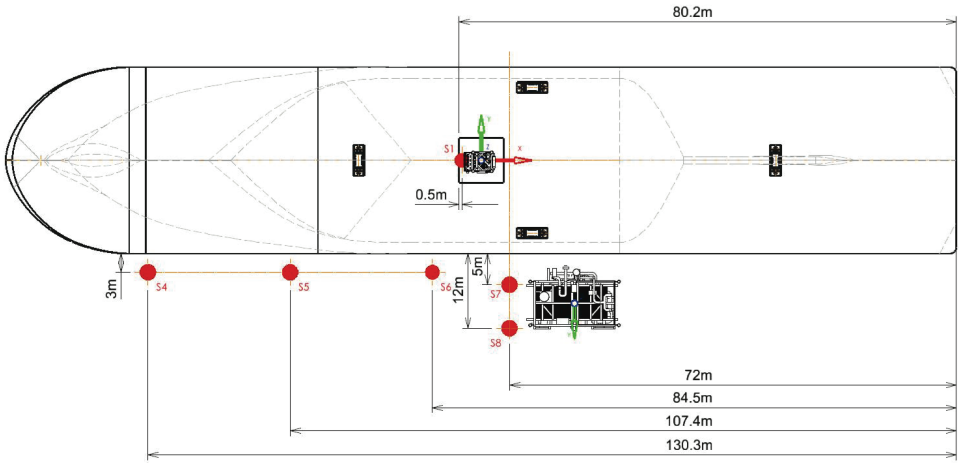

Figure 2.13: Overview of sensor locations on the model - standard size moon-pool

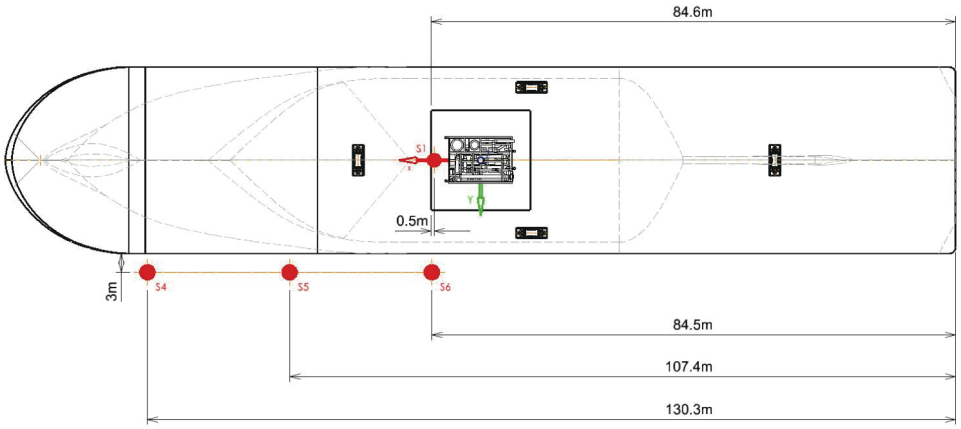

Figure 2.14: Overview of sensor locations on the model - enlarged size moon-pool

2.5 Sea-states

All the model tests were performed in irregular waves and the specter based on Torsethaugen and Haver [2004] was used to generate the waves. The Torsethaugen specter accounts for waves generated by the local wind and incoming swell from other areas. This two-peaked specter is based on readings from various locations on the Norwegian continental shelf and is considered to be a realistic realization of the sea-states in this area.

All wave runs were performed with a significant wave height of $H_S = H_{m0} = 4.5m$ and primary peak periods of $T_p = [8\ 9\ 11\ 14]s$. The processing windows were all 33 minutes in model scale in order to simulate a 3 hours wave train in full scale as calculated by equation 2.2.

2.6 Signal processing

The spectral analysis was performed in MatLab. The built in function based on Welsh's method for signal processing was used. The method is dividing the signals into so-called Hanning windows, with or without overlap, and estimating a spectrum for each window by discrete Fourier transform. Finally the individual spectra are averaged to achieve a smooth curve. In order to display a realistic spectral density function, it is a trade off between high resolution and a smooth function. Small Hanning windows give a smooth curve, while large windows will give high resolution. The best results were achieved by dividing the signal into 60 windows of equal length.

The theoretical spectra are calculated by using the Torsethaugen function provided by WAFO-group [2000].

Before the model testing was initiated, the wave realization was run in the ocean basin without models. Two wave probes were located in the water for calibration purposes. Figure 2.15 shows the spectra based on the information from the wave probes and the theoretical spectra in the same graphs. There is a good similarity between the theoretical spectra and the processed spectra. This proves that the generated waves are good realizations of the desired spectra. It also indicates that the signal processing method that is used in this thesis can be trusted to a certain limit.

It seems like the experimental spectra have in general lower values for spectral density than the theoretical ones. This can cause more uncertainties while performing analyses related to spectral moments. To check this, the significant wave height has been calculated by using Equation 2.5. The results are presented in Table 2.1 and seem to be accurate within $\pm 5\%$ of the input value of $H_S = 4.5m$. This is an acceptable error regarding the fact that

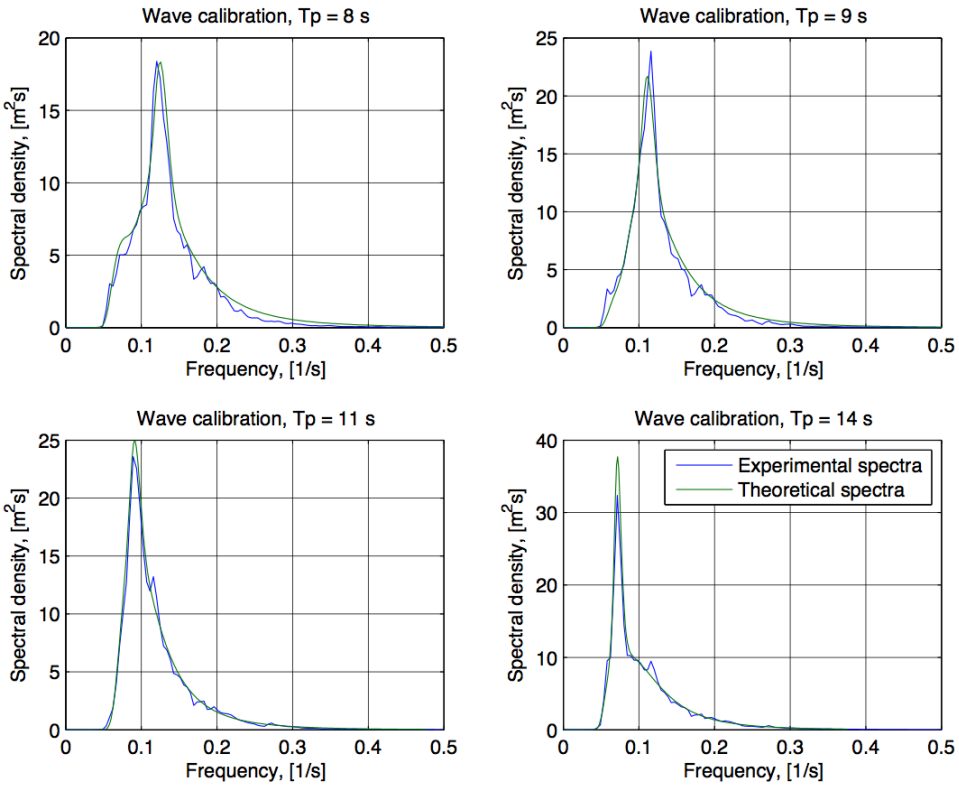

Figure 2.15: Theoretical and experimental wave spectra

is a combination of errors from the wave making process and the numerical processing of the data.

$$H_S = H_{m0} = 4\sqrt{m_0} = 4\sqrt{\sum S(f_i) * \Delta f} \tag{2.5}$$

Table 2.1: Significant wave heights

T_p **[s]**	**Experimental** H_{m0} **[m]**	**Theoretical** H_{m0} **[m]**
8	4.2927 (−4.61%)	4.5550 (+1.22%)
9	4.4403 (−1.33%)	4.5582 (+1.29%)
11	4.4307 (−1.54%)	4.5406 (+0.90%)
14	4.4138 (−1.92%)	4.5327 (+0.73%)

2.7 Model test results

2.7.1 Surface elevation specter

The specter of the surface elevation inside the moonpool is presented in Figure 2.16. This is for the specific case where the inlet-cooler module is lowered to elevation M1 (Figure 2.8) and the peak period is $T_p = 9s$. The surface elevation is found from sensor S1 (Figure 2.14) and the specter is calculated as described in section 2.6.

It is clear that the vertical motion of the vessel in this case is inertia dominated in this wave system and have little effect on the moonpool water elevation. The internal surface elevation is more dominated by the waves. It is also clear that the more high-frequent waves are eliminated inside the moonpool. That is further investigated by comparing the surface elevation inside and outside the moonpool. The specter for sensor S6 is presented in Figure 2.17. It is important to keep in mind that the vertical vessel motion alongside the ship is much more sensitive to the rolling motion than the vertical vessel motion inside the moonpool. Attempts have been made to remove the component of vessel motion in the wave probe read off, but without success. However, in the high-frequent area where $f > 0.15[1/s]$ there is no vessel response. Thus we can see that the high frequent surface elevation response is very large aside the vessel compared to inside the moonpool.

Just by looking at Figure 2.17, it is hard to explain why the high frequent response is larger than the incident waves specter. This is further investigated by looking at the video of the model testing. It is possible to observe visually the reason for those high-frequent waves. When the shortest waves hit the bow of the vessel, they grow in height alongside the vessel. It is also observed that during those waves, the moonpool elevation seems to be completely unaffected. This is reasonable regarding the fact that the surface elevation spectral density in Figure 2.16 is close to zero when $f > 0.15[1/s]$.

2.7.2 Surface elevation transfer function

The transfer function is found by using Equation 2.6. The transfer function for $T_p = 9$ and with the inlet-cooler at elevation M1 is plotted in Figure 2.18. The RAO calculated by Oceanide is plotted in the same figure as the one calculated in this thesis. It can be observed that both calculations are similar, but the calculation from Oceanide has higher resolution and deviation. That means that it is a more exact representation of the samples. But since the student analysis is smoother, it is probably a more realistic representation of the actual case.

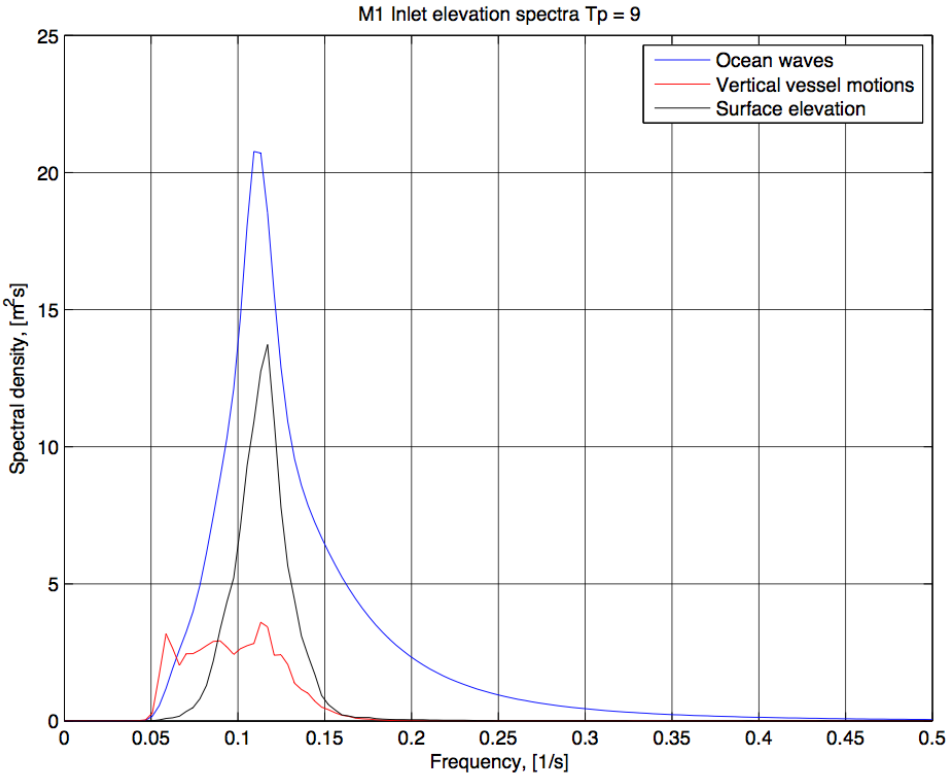

Figure 2.16: Specter of the surface elevation inside the moonpool

$$H(f) = \sqrt{\frac{S_{Response}(f)}{S_{Torsethaugen}(f)}} \tag{2.6}$$

The transfer function should be the same, no matter which sea state it is measured from. Therefore, the transfer function estimations for each sea state is plotted in the same graph in Figure 2.19. It seems like the different estimations have good similarity within the frequency interval where the spectral densities are not close to zero.

2.7.3 Surface elevation significant wave height

In order to check how the wave height inside the moonpool is sensitive to the various module elevations and wave spectra, the significant wave height is found and plotted into Figures 2.20, 2.21 and 2.22. The significant wave height is found from Equation 2.5. It is observed that for all the modules, the sea state with $T_p = 9s$ gives the largest response. Therefore, it can be

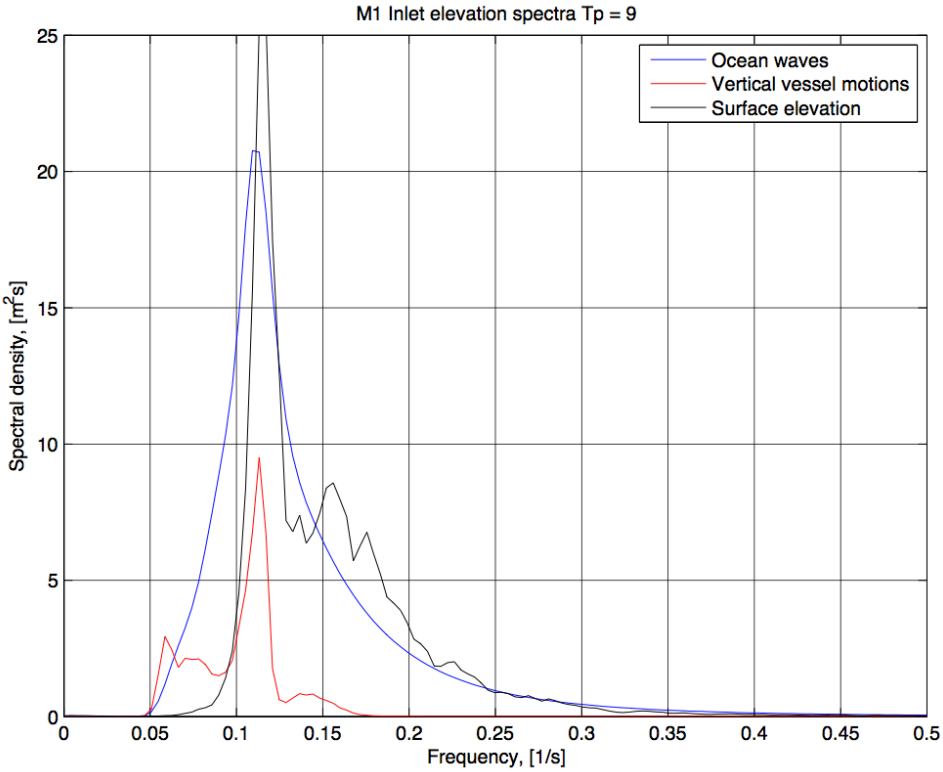

Figure 2.17: Specter of the surface elevation outside the moonpool

assumed that this sea state contains more waves of resonant frequencies than the other sea states.

Another interesting observation is that for the inlet-cooler, the significant wave height for M4 is significantly larger than for the other elevations. A possible explanation for that is that the projected area for the inlet-cooler is larger than for the compressor. This means that the module is blocking the waves from entering the moonpool. But when the module is at its lowest elevation M4, it is out of the way for the waves and they can enter the moonpool freely. This explanation is backed up by the observation that the significant wave height for M4 is similar to the ones for the narrower compressor module. The compressor module will allow water to flow more freely for all elevations.

For the pump module, which is lowered through the standard size moonpool, the results are not that different from the results found for the enlarged size moonpool. They are a little lower, but not to a level so distinct that we can say anything about the difference between the different moonpool sizes.

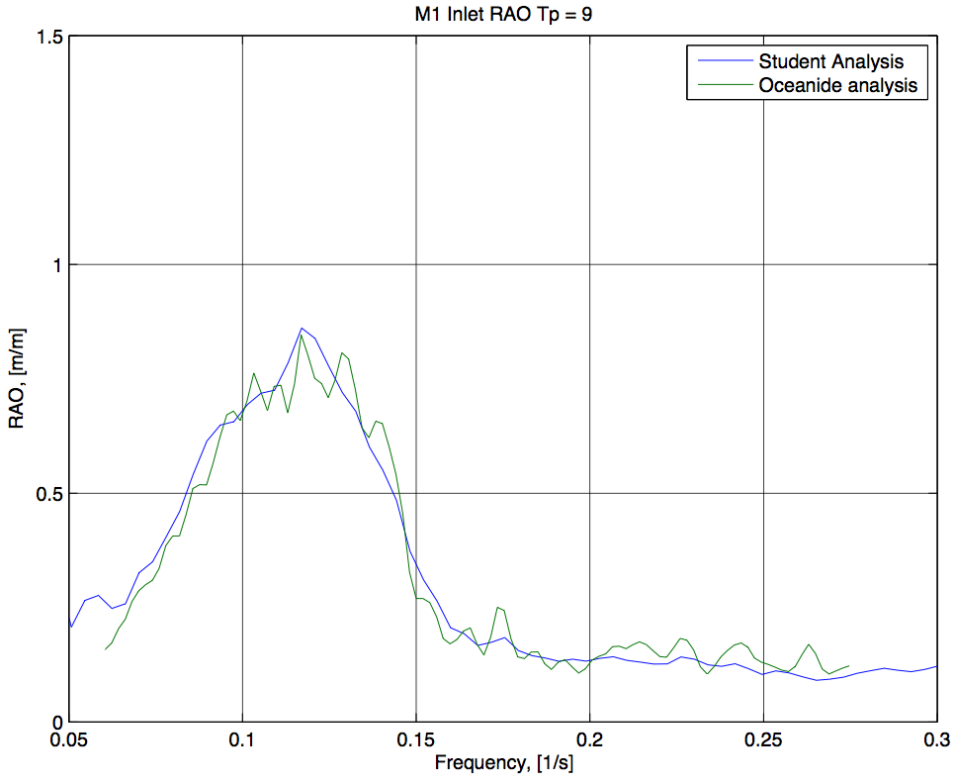

Figure 2.18: Transfer function of surface elevation inside moonpool

2.7.4 Vertical force on module

The 6 DOF transducer, mounted on the ship model, measure the vertical force. The measured total force consists of hydrodynamic forces acting on the model and the inertia force due to the mass of the module and the motion of the vessel. For this thesis the inertia contribution is excluded by subtracting it from the total measured force.

The statistics for the force is calculated the same way as for the surface elevation except for the result for significant wave height. It is divided by two so that the result is the significant force amplitude. The force specter for the inlet-cooler at elevation M1 at the sea state where $T_p = 9s$ is plotted in Figure 2.23 and the significant forces are plotted in Figure 2.24 through Figure 2.27.

Not surprisingly, the force specter is shaped very similar to the surface elevation specter. This indicates that the force is primarily driven by the surface elevation inside the moonpool.

For the modules inside moonpools, the significant force is clearly lowest when

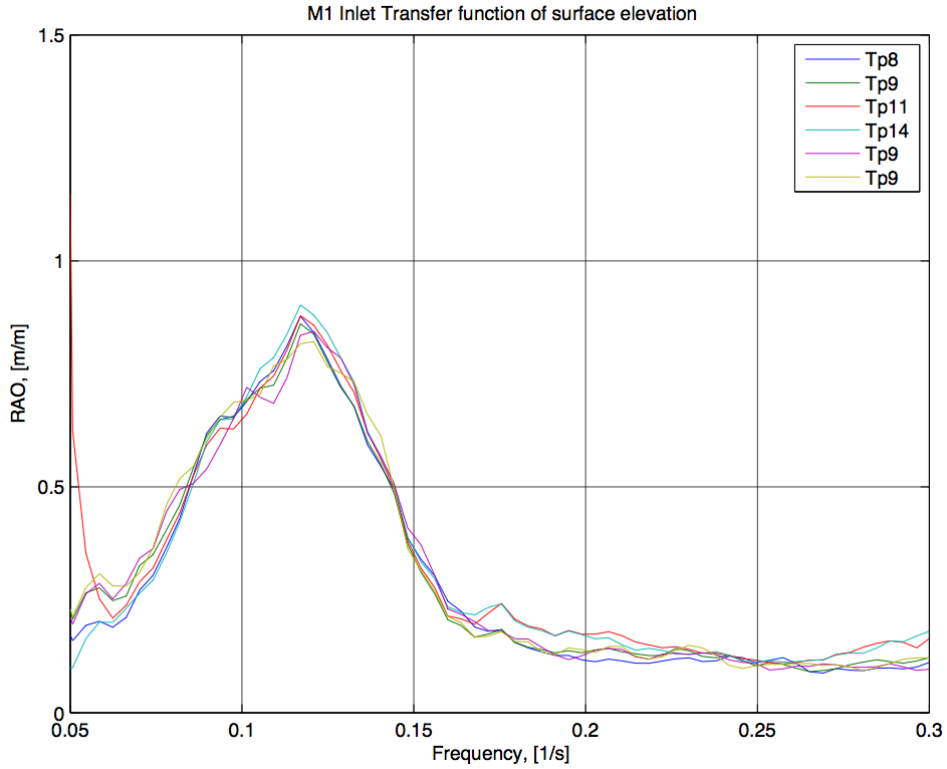

Figure 2.19: Transfer function of surface elevation inside moonpool for all sea states

the module is at the lowest elevation. That makes a lot of sense since the flow is less restricted when the module is under the moonpool instead of inside. Another observation is that the force also is lower at the highest elevation. At this elevation, the modules are not fully submerged and have less wetted surface area. Therefore, a possible explanation to the reduced force is that the drag force is reduced when the wetted area is reduced.

From this, we can say that the vertical force acting on the modules is reduced when they pass through the moonpool. An explanation for that is that when the flow is restricted and has to squeeze past the module. When the module is located below the vessel hull, the water flowing in and out of the moonpool will spread more sidewise past the module and not only up and down.

The significant force on the inlet-cooler lowered aside the vessel in Figure 2.27 is clearly a lot larger than for the moonpool case. It is however more interesting to compare the RAO for the two cases. In Figure 2.28 we see that for the lower frequencies, the forces are a little larger inside the moonpool. While for the higher frequencies, the force is significantly largest outside the moonpool. This proves that the low frequent waves are shielded inside the

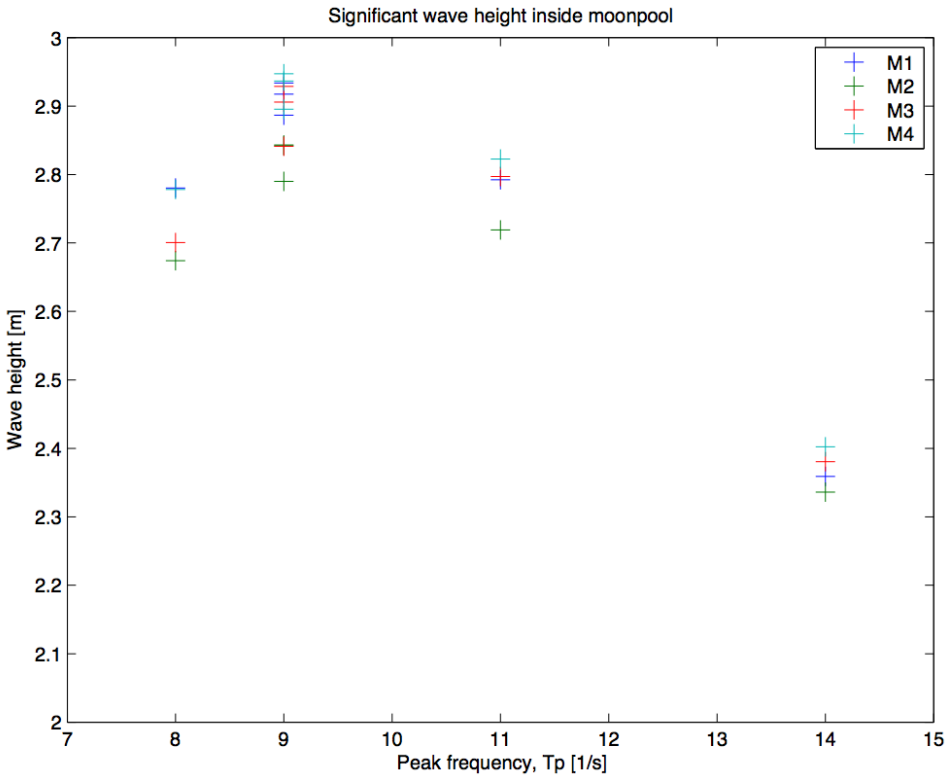

Figure 2.20: Significant wave height inside moonpool with compressor module at various elevations

moonpool while the low frequent waves are slightly amplified. According to theory we could expect a resonant response inside the moonpool a lot larger than what we can observe outside the moonpool. There are no good indications of such an effect, which is probably caused by the complexity of the entire system and large amounts of damping.

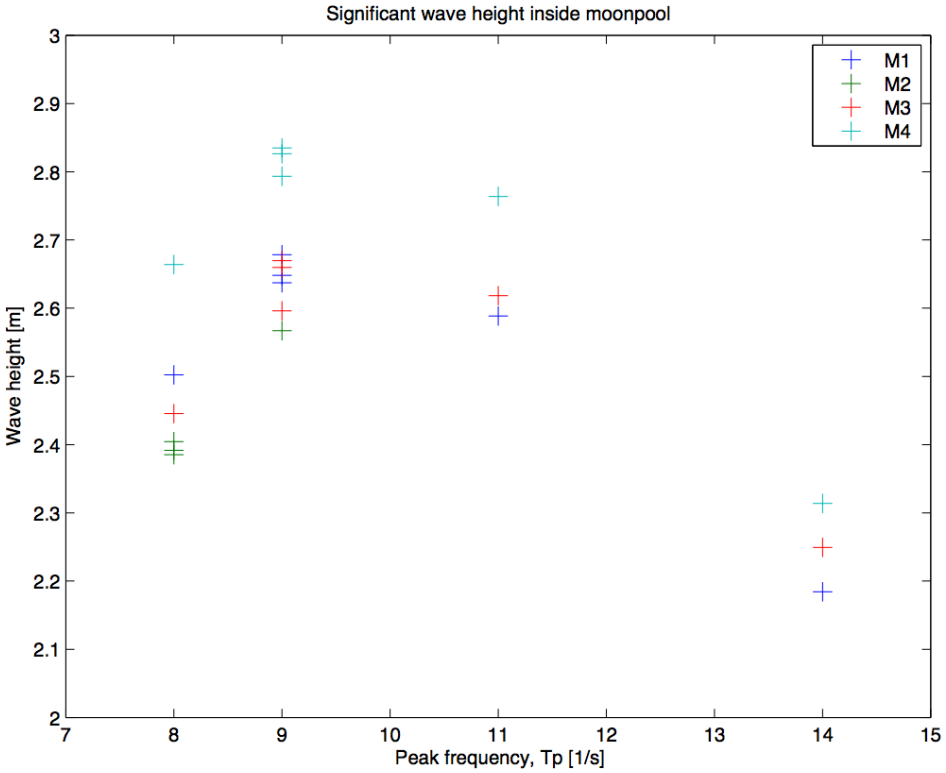

Figure 2.21: Significant wave height inside moonpool with inlet-cooler module at various elevations

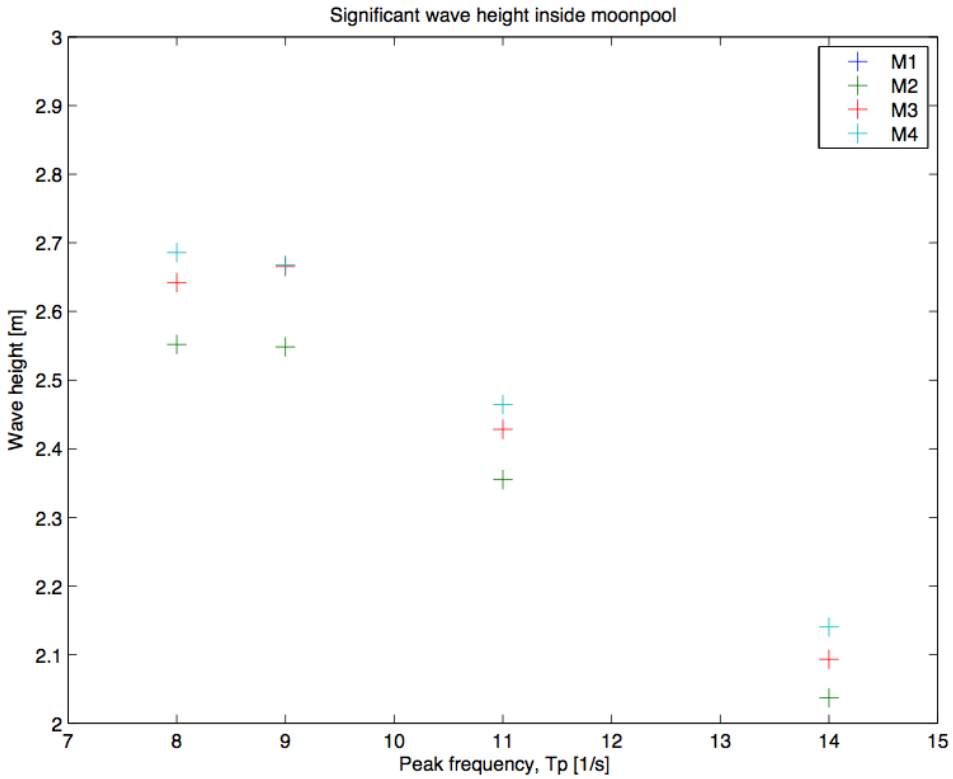

Figure 2.22: Significant wave height inside moonpool with pump module at various elevations. (The wave probe was not properly connected for M1)

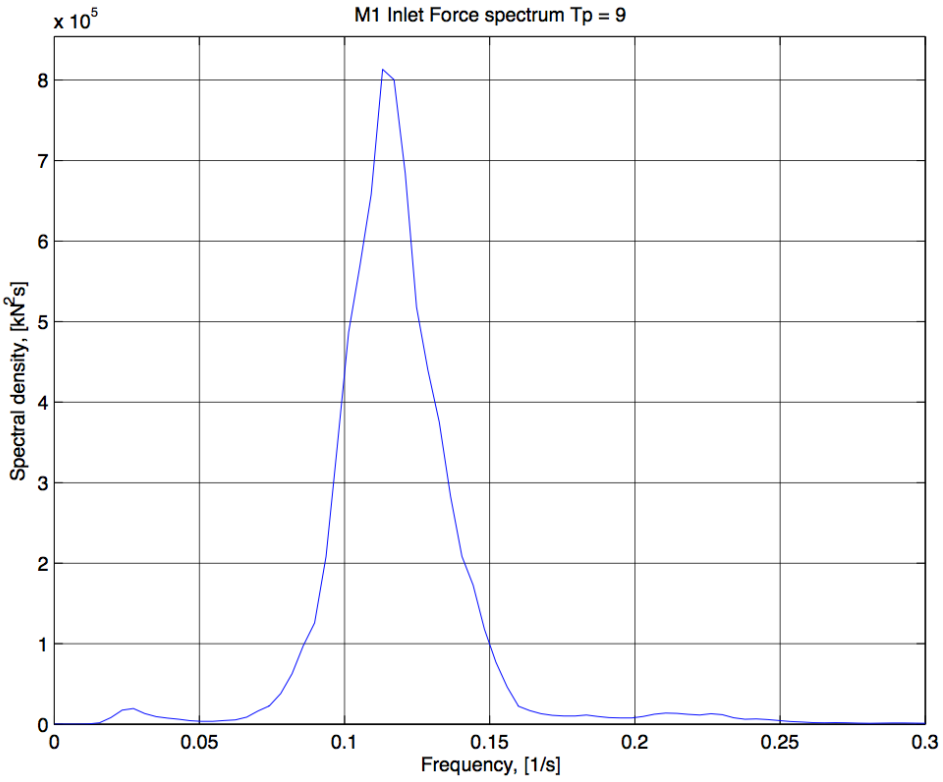

Figure 2.23: Spectral density for vertical force on module

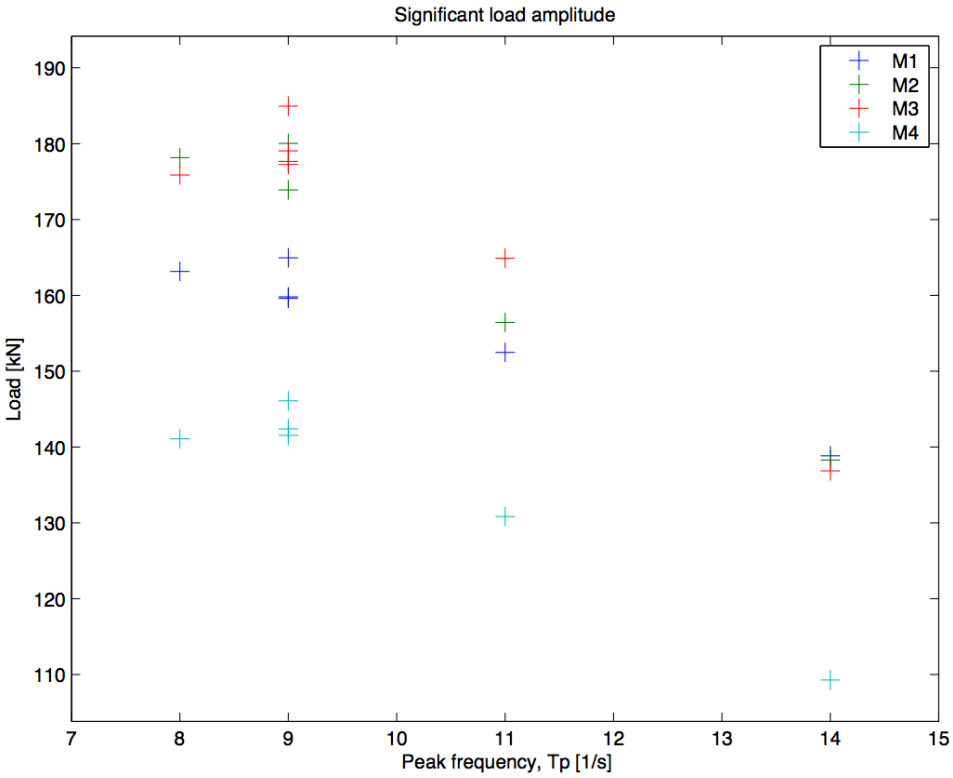

Figure 2.24: Significant force on compressor module at various elevations

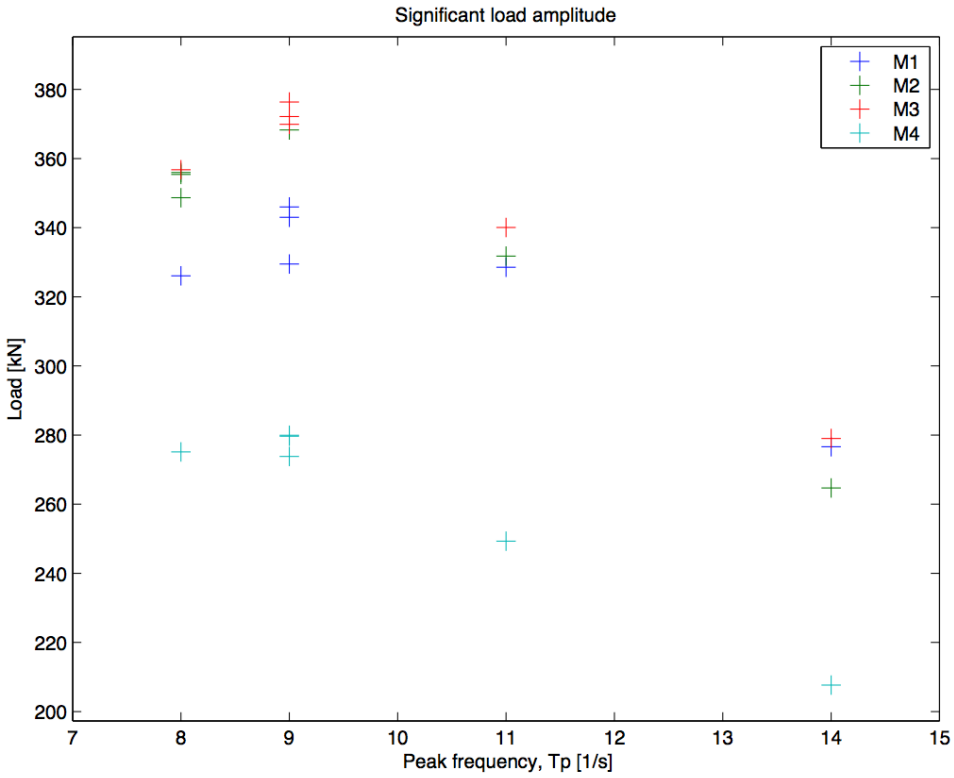

Figure 2.25: Significant force on inlet-cooler module at various elevations

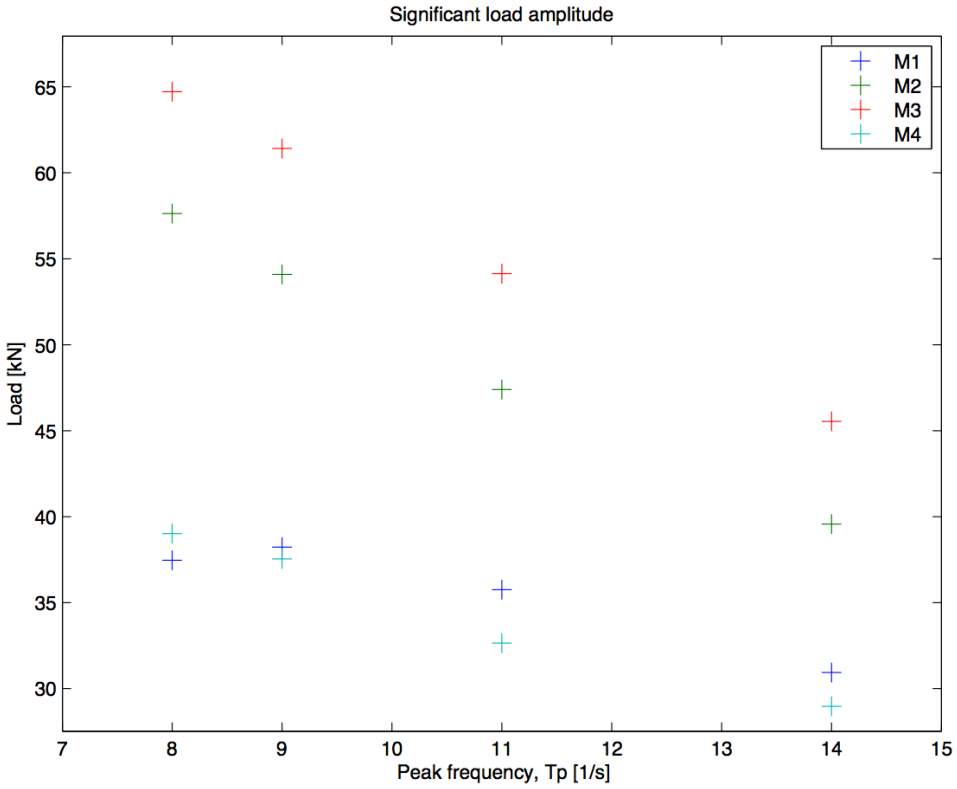

Figure 2.26: Significant force on pump module at various elevations

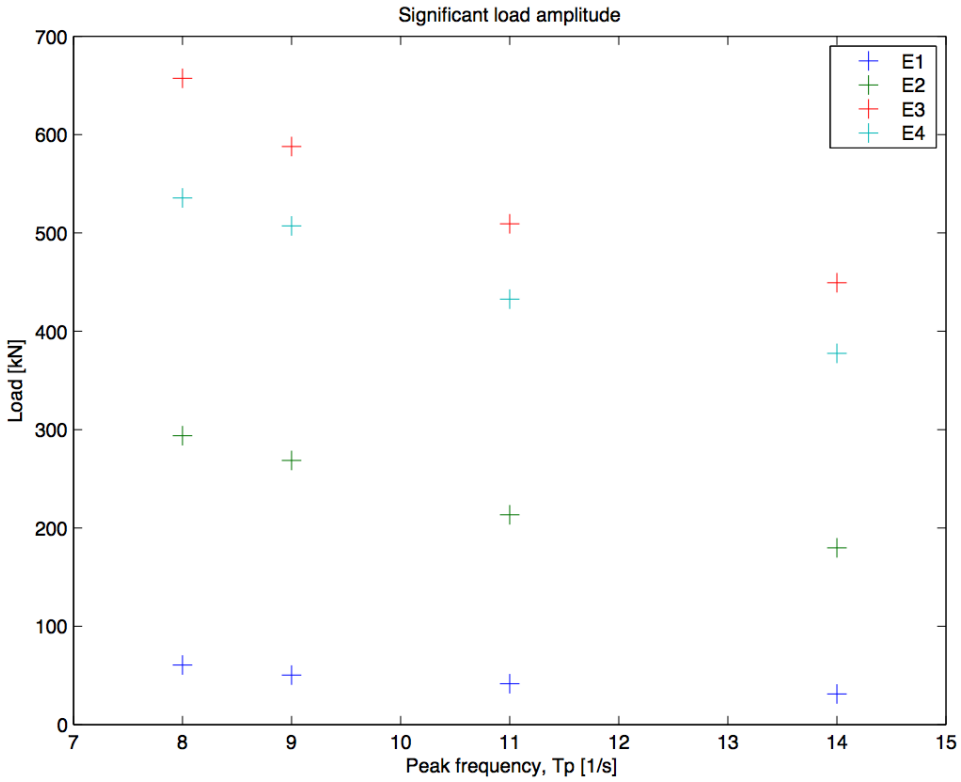

Figure 2.27: Significant force on inlet-cooler module at various elevations aside the vessel

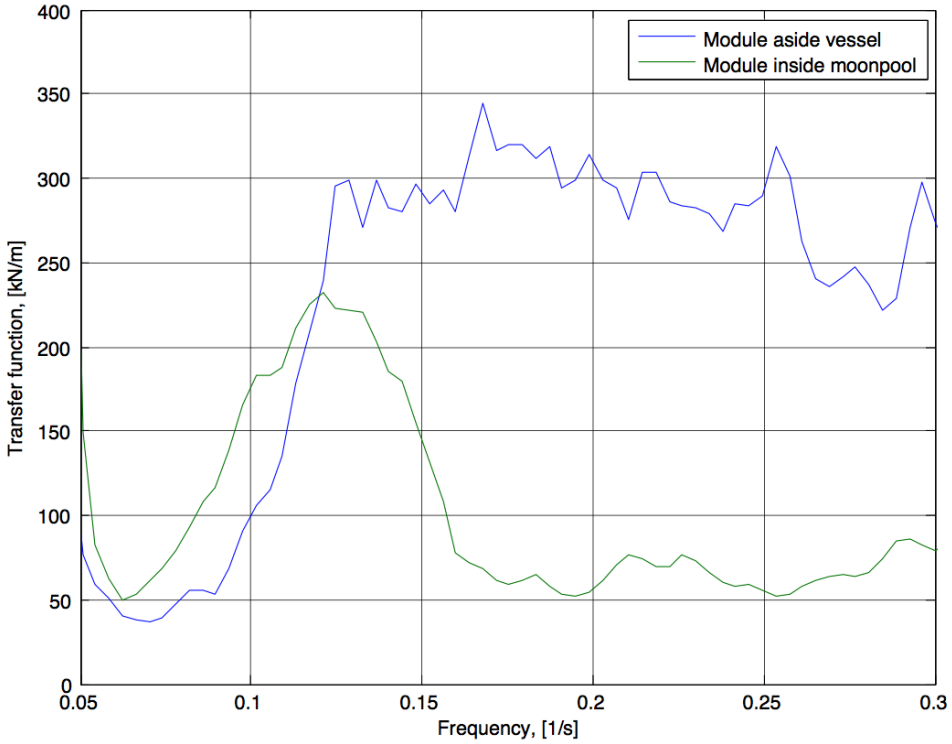

Figure 2.28: Significant force on inlet-cooler module at various elevations aside the vessel

Chapter 3

Numerical analysis

The goal of this numerical analysis is to reproduce the results from the model testing. If there is found a good match between the experimental and numerical results, the accuracy of the numerical model can also be trusted for similar cases. Then the numerical model can be used to investigate the effects of changing the size of the moonpool.

In Technip Norge, OrcaFlex is used for most operational analyses. Since the software and a lot of competence in using it is available, it is desired to use OrcaFlex to perform the analyses in this thesis. OrcaFlex can be used to simulate a full lowering operation through the splash zone in time domain. OrcaFlex does not account for disturbance in the water caused by structures. Therefore, OrcaFlex alone will not solve the effect of shielding, piston and sloshing modes. These effects can however be included by importing results from potential solvers such as WAMIT. The results needed are so called sea state disturbance RAOs. Briefly that is velocity potential disturbance RAOs measured relative to the undisturbed waves. These RAOs are evaluated for a selection of user defined coordinates in the fluid space for the required wave headings and frequencies.

3.1 WAMIT

"WAMIT is a radiation/diffraction program developed for the analysis of the interaction of surface waves with offshore structures. WAMIT is based on a three-dimensional panel method." (Mas) The flow is assumed to be potential without any separation and lifting effects.

When WAMIT runs the analysis, the two subprograms POTEN and FORCE are usually run sequentially as shown in Figure 3.1. GDF and FRC are input files required to run POTEN. GDF defines the geometry of the structures

while POT defines all the other input values such as wave headings and frequencies. POTEN solves the velocity potential for radiation and diffraction and stores the results in the binary file P2F. P2F is together with FRC the required input files to run FORCE. FRC defines the points in the fluid domain to be evaluated by FORCE. FORCE computes the global quantities such as hydrodynamic coefficients, motions and forces. Since the output from POTEN is stored in P2F, it is possible to make several runs with FORCE, altering the requested parameters, without having to re-run POTEN. This is very beneficial since POTEN usually requires a lot more computation time.

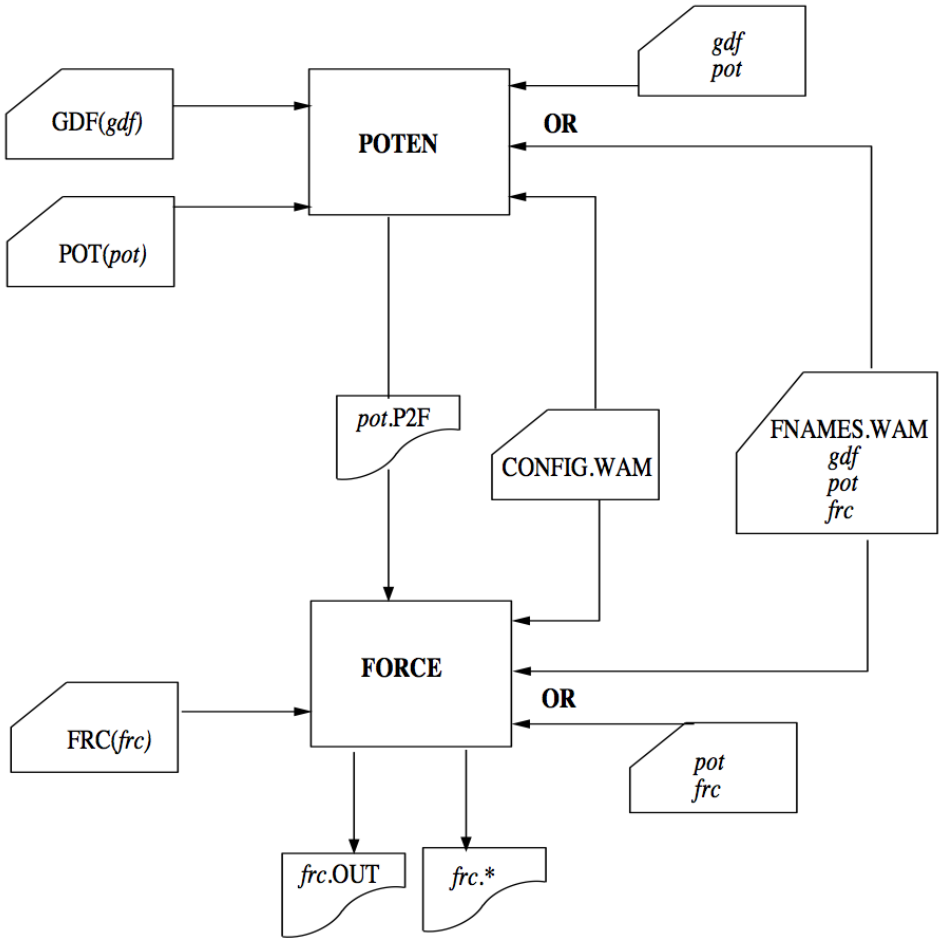

Figure 3.1: Flow chart of WAMIT showing the subprograms POTEN and FORCE with their associated input and output files

3.2 Modeling of the North Sea Giant

The North Sea Giant is modeled using Multisurf. The benefit of using Multisurf is that it has the option to define panels and export them to WAMIT input files.

The vessel was first modeled without moonpool as shown in Figure 3.2. It is only necessary to model the wetted surface of the vessel. In this case, the water surface level is defined to be the plane $z = 0$. WAMIT will automatically detect the panels that are adjacent to the free surface.

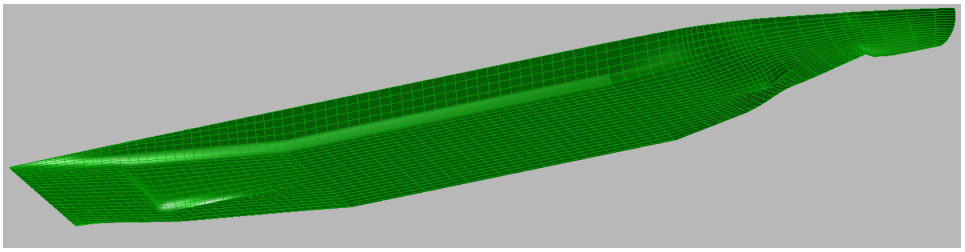

Figure 3.2: Model of the wet surface of the North Sea Giant showing the distribution of panels

The shape of the hull is modeled by defining points found from the vessels general arrangement drawing and assigning curves to those points as shown in Figure 3.3. These curves are then used to define patches to represent parts of the hull such as Figure 3.4 representing the bow.

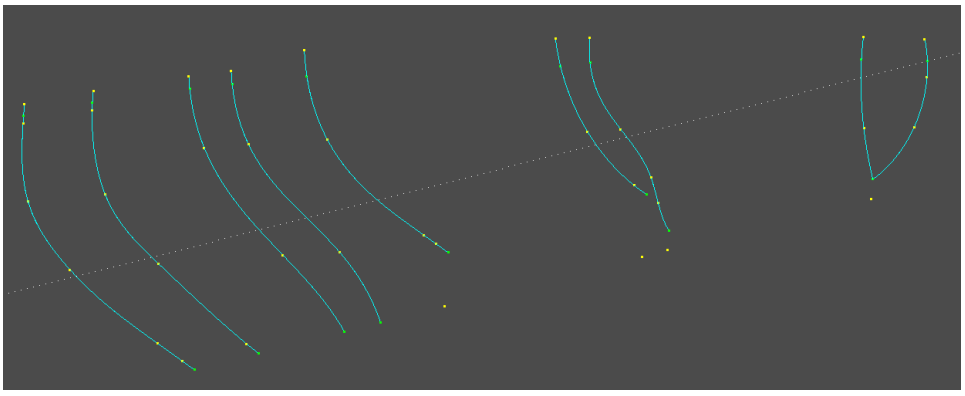

Figure 3.3: Curves used to define the bow

A lot of care had to be taken while defining the sizes and concentration of the panels. In order to best represent the geometry, it is essential to ensure that the panels are concentrated around details. However, this concentration must also be properly adapted to the rest of the model. If we compare Figure

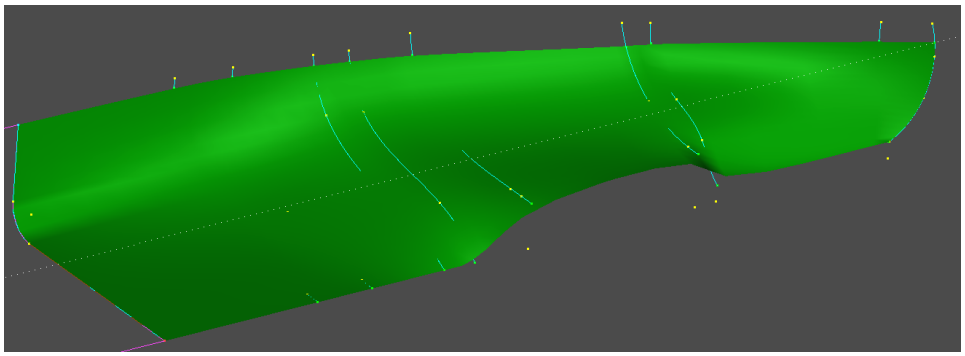

Figure 3.4: The patch defining the bow

3.5 and Figure 3.6, we observe that the geometry of the model is smoother and more realistic when the distribution is properly adapted.

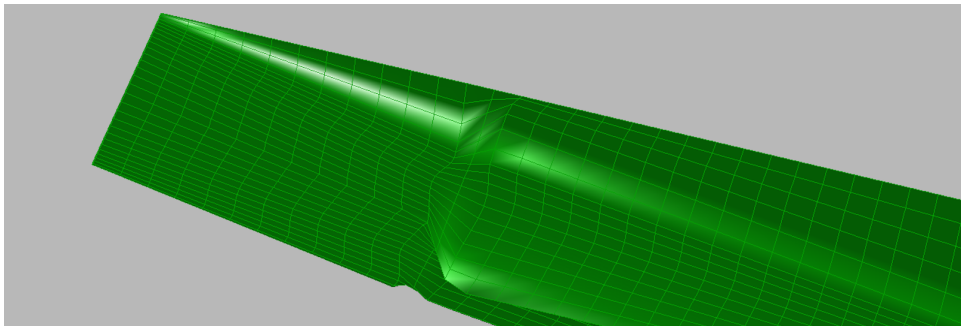

Figure 3.5: Stern with even distribution of panels

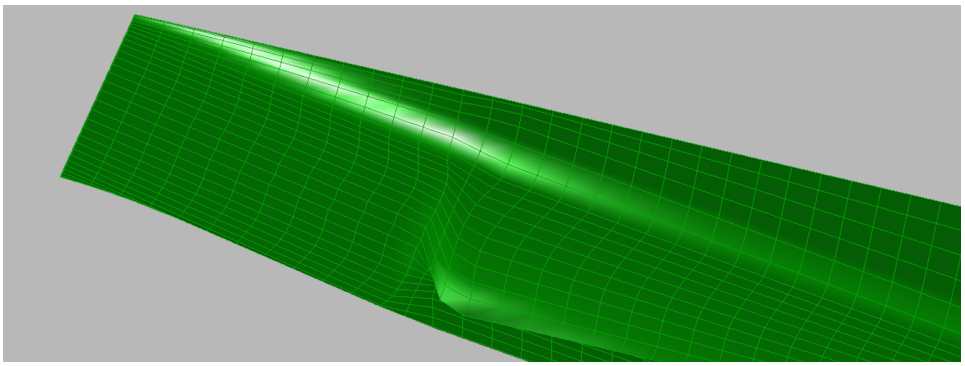

Figure 3.6: Stern with adapted concentration of panels

3.3 Moonpool modeling

The moonpool is modeled as shown in Figure 3.7 for the standard size moonpool and Figure 3.8 for the enlarged size moonpool. It was challenging to get the panels along the moonpool walls to match properly to the panels along the hull. Therefore triangular elements were chosen to represent this part of the hull.

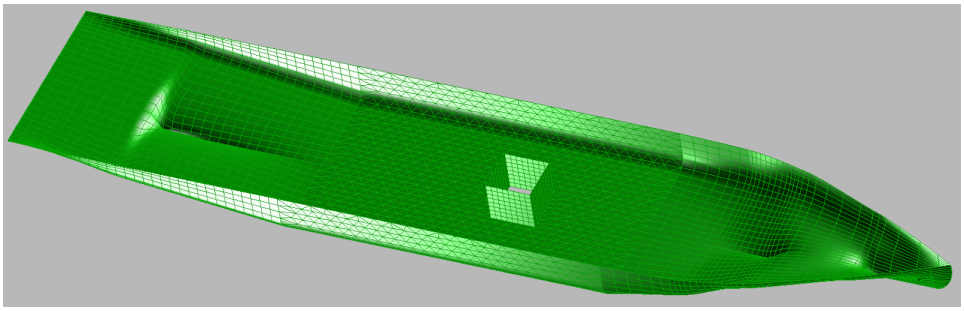

Figure 3.7: Ship model with standard size moonpool

The solid inside the moonpool in Figure 3.9 is not representing a structure. It defines points in the fluid domain where the pressure and velocity are going to be computed for. This is the information that is going to be imported into OrcaFlex. The solid extends from the water surface and down to $5m$ under the keel.

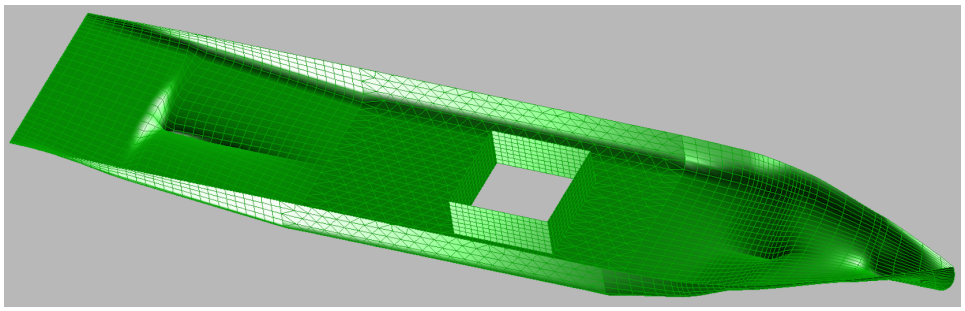

Figure 3.8: Ship model with enlarged size moonpool

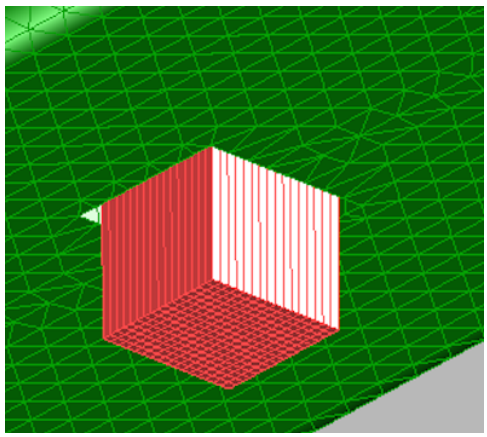

Figure 3.9: Ship model with enlarged size moonpool

3.4 Surface elevation RAO

Sea state disturbance RAOs are based on the output from WAMIT and adapted to OrcaFlex format by the OrcaFlex import function. The actions of this function are described in the document attached as Appendix A. Sea state disturbance RAOs are the amplitudes of the velocity potential in relation to the incident undisturbed waves. In order to find the surface elevation RAO, the z-component of the sea state disturbance RAO for all points on the water surface is read and presented by a Matlab script. The results presented here are all for a vessel heading of 15°. The surface elevation amplitude is only displayed for the relevant resonant frequencies.

Figure 3.10 shows the piston mode for the standard moonpool. The magnitude of the amplification of about 5.4 is clearly the largest to be found in the numerical analysis. It has occurred at a period of 6.1s. This is less than what was expected according to Molin [2001] calculations, as described in Figure 1.3. However, it is not surprising since Molin [2001] did his studies in 2D while this is a 3D analysis.

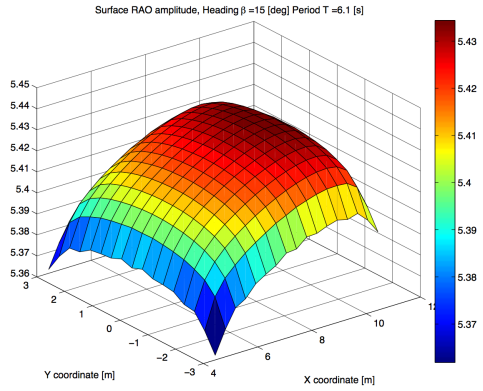

Figure 3.10: Piston mode surface elevation RAO for standard size moonpool

Figure 3.11 shows the first sloshing mode for the same moonpool. The magnitude is a lot lower than for the piston mode. Another aspect to bear in mind is the fact that the wave period for for this condition to occur is only 3 seconds. If we look at the graphs in Figure 2.15, it is clear that the amount of energy for a wave period of 3 seconds is very low for all the considered sea states. This makes the first sloshing mode even less critical for the standard size moonpool.

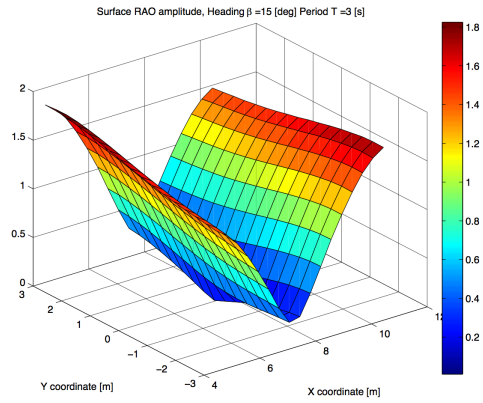

Figure 3.11: First order sloshing mode surface elevation RAO for standard size moonpool

When the moonpoool is enlarged, one should according to Figure 1.3 expect that the sloshing modes would become more dominant than for the standard size moonpool. Looking at Figure 3.12 it is clear that the amplification is heavily reduced compared to the standard moonpool. The amplitude is only increased by about 15% in relation to the incident wave. Knowing this it is reasonable to state that the effect of the piston mode is significantly reduced when the moonpool size is enlarged.

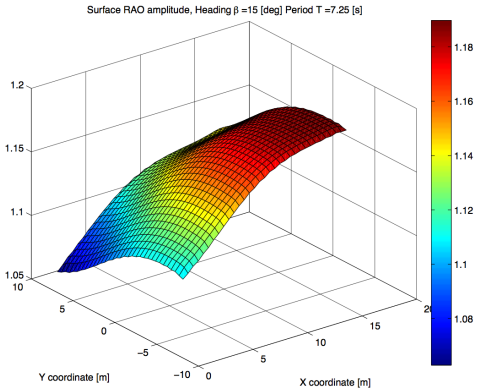

Figure 3.12: Piston mode surface elevation RAO for enlarged size moonpool

Considering the resonant period first order sloshing mode in Figure 3.13, it clearly occurs in a domain with a lot more energy present than for the standard moonpool. The amplification of about 20% more than the incident wave is not very large, but should not be disregarded. There is a large section in the middle of the moonpool where the wave elevation is cancelled. This cancellation is an important characteristic for sloshing.

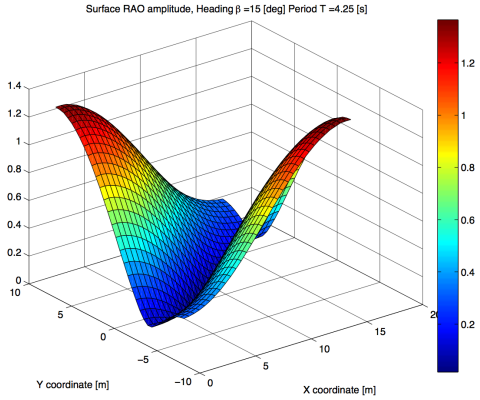

Figure 3.13: First order sloshing mode surface elevation RAO for enlarged size moonpool

Figure 3.14 is very interesting. We can observe second order sloshing in the vessels transverse direction, while we observe first order sloshing in the longitudinal direction. The amplification of over 3 is of great significance. However, the amount of energy in the considered sea states is low for a wave period of only 3 seconds.

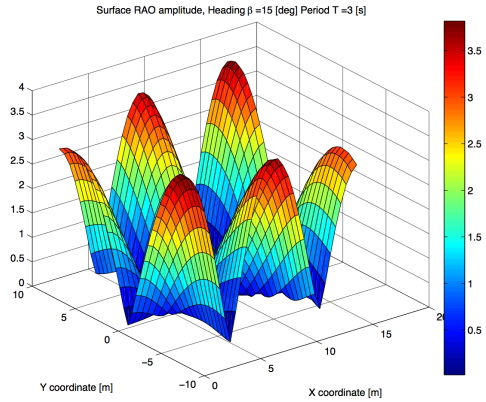

Figure 3.14: First and second order sloshing mode surface elevation RAO for enlarged size moonpool

3.5 Added mass and damping

In order to figure out how the added mass and damping coefficients for a module inside the moonpool is affected by being in a moonpool, a multi-body analysis was run in WAMIT. The run was performed for the standard size moonpool since the piston mode is most critical for that moonpool and will probably trigger some reaction. The module is simply shaped as a shoebox with dimensions $4m * 4m * 4m$. The module is located in the center of the moonpool with the top piercing through the water surface as can be seen in Figure 3.15. Physically this will represent a module that is somewhat taller than $4m$ but with a $4m$ draft. Meaning that any effects that would be represented by the top of the module will not be included.

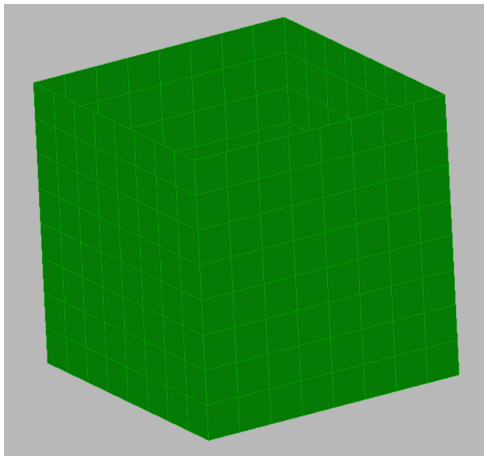

Figure 3.15: Box used as module

In Faltinsen [2005], the added mass and radiation of a catamaran is referred to. Figure 3.16 is the amplitude of the radiated waves in terms of the non-dimensional forced heave frequency. The radiated waves are related to the damping according to equation 3.1

$$b_{33} = \frac{\rho g^2}{\omega^3} \bar{A}_3^2 \tag{3.1}$$

where b_{33} is the damping in heave caused by heave motion and $\bar{A}_3$ is the amplitude of the radiated wave.

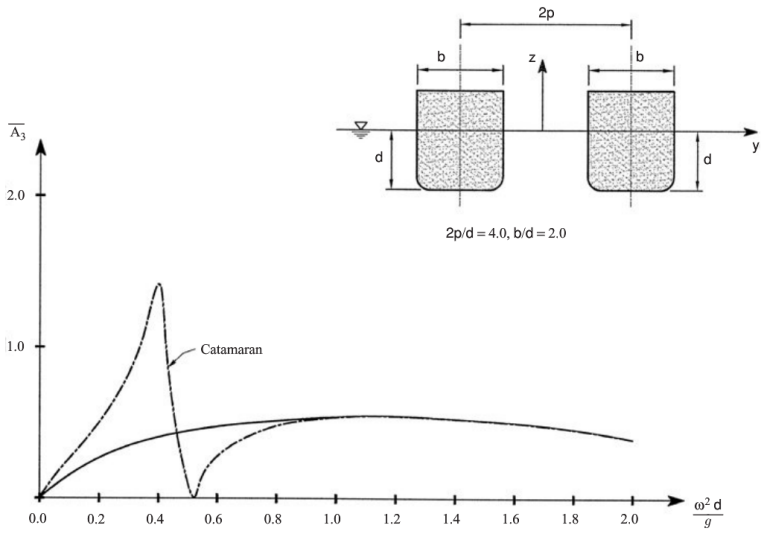

Figure 3.16: Amplitude of heave-induced radiation waves

In Figure 3.17, the added mass is presented in terms of the same non-dimensional frequency as for the radiation. It is important to note that these are results for a the heave motion of the vessel itself and not for a module inside the moonpool. Therefore the results should not be equal, but at could explain some trends.

Figure 3.18 and 3.19 shows the added mass in heave of the box module in terms of the non-dimensional frequency. Results for the module inside the moonpool are compared to the results for the module in open water. We can observe that for higher and lower frequencies the added mass converges towards similar values. However, for the frequency related to the piston mode, the added mass is very large, and then very low with a negative value. The negative section can be explained by comparing to the catamaran result in Figure 3.17. The positive section cannot be explained by the catamaran results. It does not go to infinity, so it is probably related to something

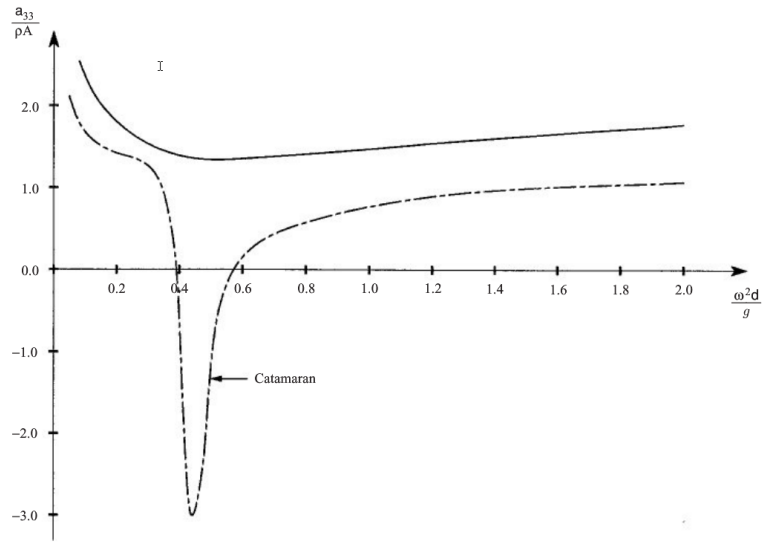

Figure 3.17: Added mass for catamaran in heave

physical. It could be a three dimensional effect, or it could be related to some vessel response.

Figure 3.20 and 3.21 shows the damping of the module inside the moonpool and in open water. In general, the damping is reduced compared to the open water. But for the piston mode frequency, the damping is significantly increased. We can observe a fair correlation with Figure 3.16, at least for lower frequencies. The section where the damping increases with increasing frequency and suddenly drops to zero is very similar. For higher frequencies, the module damping remains at the zero level, while the catamaran radiation increases. This can be justified with the fact that it is outside the resonant region and the fact that the cases are different.

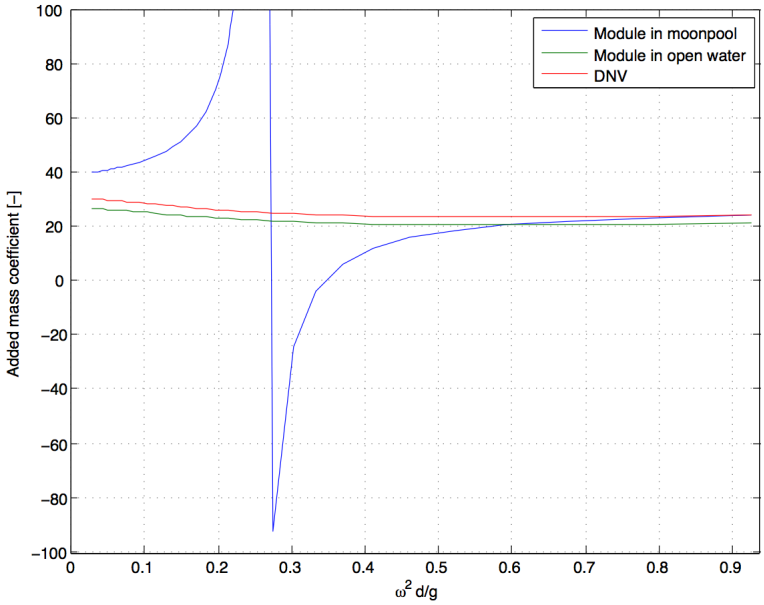

Figure 3.18: Added mass coefficient in heave for module in open water and inside moonpool

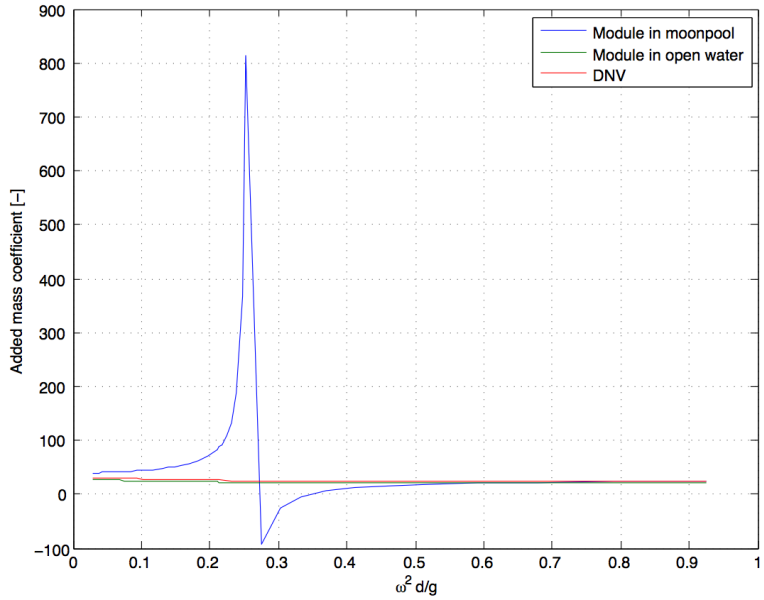

Figure 3.19: Added mass coefficient in heave for module in open water and inside moonpool

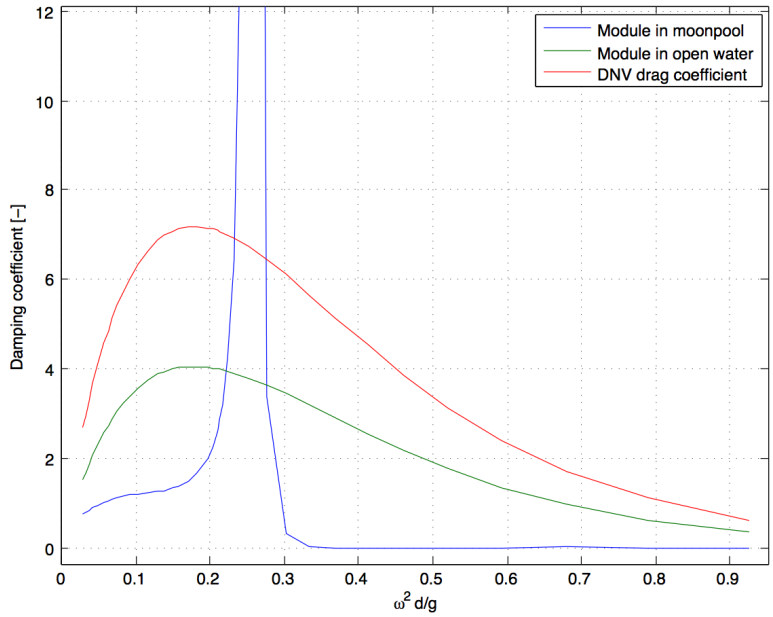

Figure 3.20: Damping coefficient in heave for module in open water and inside moonpool

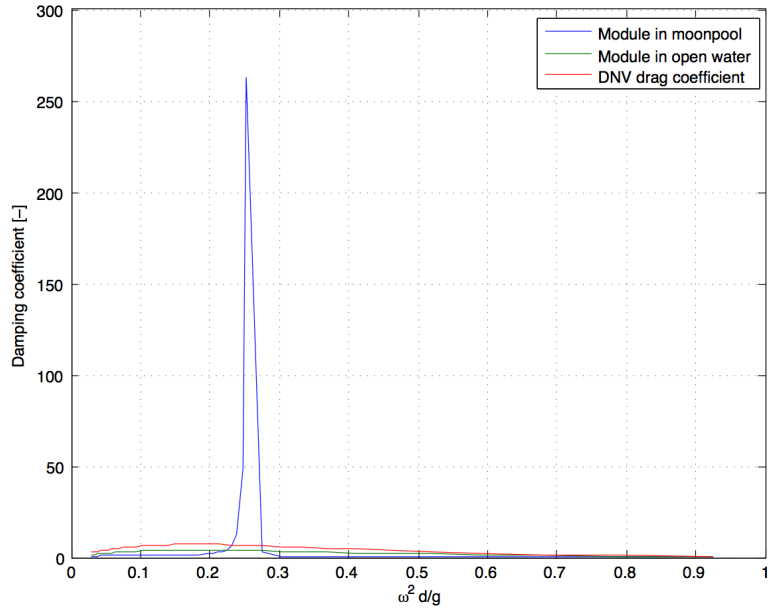

Figure 3.21: Damping coefficient in heave for module in open water and inside moonpool

Conclusion and further work

Conclusion

The model test campaign studied in this thesis was intended for analysis of one very specific lowering operation. The modules and the vessel are all complex structures. There are a lot of details to consider and it has proven to be very difficult to reproduce the data from the model testing. If the model tests were intended for more scientific investigations of moonpool effects, a more generic approach would have been chosen.

However, the model tests prove that there is a great advantage of lowering modules through moonpools. The modules are especially shielded for the waves of the highest frequencies, which allow the lowering operation to be performed with reduced loads and improved level of safety.

The numerical results are indicating more aspects related to moonpool hydrodynamics. The piston mode causes an extreme amplification for the standard size moonpool. This result is not realistic due to the limitations from potential theory. Since potential theory assumes inviscid flow, a lot of damping effects are not included such as friction along the moonpool walls and flow separation. For the enlarged moonpool, there is also a piston mode. But the amplification is heavily reduced compared to the standard size moonpool. It is reasonable to claim that the amplification will be further reduced due to the viscous effects. The piston mode can therefore be considered to be of less importance for the enlarged moonpool.

On the other hand, the sloshing modes will be more likely to occur for the enlarged moonpool. This is based on the fact that the resonant period for first order sloshing is longer for larger moonpools. Therefore the sloshing mode will be within a frequency range with more energy than it would be for a smaller moonpool. It is however important to note the shape of the surface during the sloshing modes. The peaks are primarily located adjacent to the walls. This is not very realistic because of the viscous effects close to the walls. If additional friction is accounted for, the peaks should be located a little further away from the walls and be of less magnitude.

Based on this information, we can conclude that when the moonpool is significantly enlarged, the resonant responses are of less importance. Sloshing will however become more dominating and should be accounted for.

Further work

First of all: The model test campaign seems to be executed well and with great relevance for the project it was intended for. But some changes would make the results more applicable for this thesis. The peak of the surface elevation can be located at various locations in the moonpool. Therefore it would be beneficial to have multiple wave probes in the moonpool in order to better be able to track the different resonant modes. More tests could also have been performed without module inside the moonpools to avoid the blocking effect given by the module. One module should also be lowered through both moonpools so that the two moonpools could be compared. There is a lot of uncertainty related to the results based on spectral analysis; the Fourier transform is not smooth enough. This would be avoided by performing the tests in regular waves.

For the first order sloshing mode, the amount of water flowing upwards equals the amount of water flowing downwards. In theory, this will cause the total flux of water flowing in/out of the moonpool to be zero at all times. It would be interesting to investigate weather or not this will cause horizontal flow inside the moonpool, especially for deep moonpools. If this is true, there will also be less flow close to the moonpool walls especially close to the bottom of the moonpool. In such a situation the effect from the suppression devices will be reduced. Therefore it would be interesting to investigate the horizontal forces inside the moonpools and check if the suppression devices are more or less efficient for different sizes of moonpools

The resonant effects are heavily reduced for the enlarged moonpool. But the moonpool is extremely large. Therefore it would be interesting to make more numerical analyses with more moonpool sizes. This way it could be possible to find an 'optimal' moonpool size.

The results from WAMIT were imported to OrcaFlex, but no OrcaFlex simulations were performed. If this was done in time domain for the same environmental condition as the model test was performed, the numerical results would probably be more similar to the experimental results.

References

DNV-RP-H103 Modelling and Analysis of Marine Operations. DNV, April 2011.

Odd M. Faltinsen. *Hydrodynamics of High-Speed Marine Vehicles*. Cambridge University Press, 2005.

Odd M. Faltinsen and Bjørn Sortland. Slow drift eddy making damping of a ship. *Appl. Ocean Res.*, 9(1):37–46, 1987.

Odd M. Faltinsen, Olav F. Rognebakke, and Alexander N. Timokha. Two-dimensional resonant piston-like sloshing in a moonpool. *Journal of Fluid Mechanics*, 575:359–397, march 2007.

Guilhem. Gaillarde and Anke. Cotteleer. Water motion in moonpools - empirical and numerical approach. *ATMA - Association Technique Maritime et Aeronautique, Paris, France*, 2004.

O. Kimmoun and B. Molin. Analyse des essais d'extinction du mode piston dans la baie de forage. Technical report, CCI Marseille - Provence Groupe ESIM, 2000.

Trygve Kristiansen. *Two-Dimensional Numerical and Experimental Studies of Piston-mode Resonance*. PhD thesis, Norwegian University of Science and Technology, Department of Marine Technology, 2009.

WAMIT user manual. Massachusetts Institute of Technology, version 6.4 edition.

B Molin. On the piston and sloshing modes in moonpools. *Journal of Fluid Mechanics*, 430:27–50, March 2001.

Oceanide. Model test report with vessel. Technical report, Oceanide, 2013.

Sverre Steen and Knut Minsaas. *TMR 4220 Naval Hydrodynamics - Ship Resistance*. Department of Marine Technology, 2012.

Knut Torsethaugen and Sverre Haver. Simplified double peak spectral model for ocean waves. May 2004.

WAFO-group. *WAFO - A Matlab Toolbox for Analysis of Random Waves and Loads - A Tutorial*. Math. Stat., Center for Math. Sci., Lund Univ., Lund, Sweden, 2000.

Appendices

Appendix A

OrcaFlex Import of Sea State Disturbance RAOs from WAMIT

OrcaFlex Import of Sea State Disturbance RAOs from WAMIT

This document gives details of how OrcaFlex imports sea state disturbance RAOs and their gradients from a WAMIT output file.

1 Summary

Essentially what OrcaFlex does is:

1. Read the pressure RAOs from the WAMIT *.out* file. Except for a non-dimensionalising scaling factor this is equal to the disturbed velocity potential, ϕ_d. OrcaFlex then calculates the undisturbed velocity potential, ϕ_u. The disturbance RAO, $\mathcal{P}$, is then simply given by $\mathcal{P} = \frac{\phi_d}{\phi_u}$.
2. Read the velocity RAOs from the WAMIT *.out* file. Except for a non-dimensionalising scaling factor this is equal to the gradient of the disturbed velocity potential, $\nabla\phi_d$. OrcaFlex then calculates the gradient of the disturbance RAO, $\nabla\mathcal{P}$, using the equation $\nabla\mathcal{P} = \frac{\nabla\phi_d - \mathcal{P}\nabla\phi_u}{\phi_u}$ (this last equation is derived below, by differentiation of the equation for $\mathcal{P}$ above).

2 Details

The velocity potential associated with a wave component of angular frequency ω and direction β, $\Phi(\mathbf{x}, t)$, can be expressed in terms of a complex velocity potential RAO, $\phi(\mathbf{x})$, as:

$$\Phi(\mathbf{x}, t) = \Re\left\{\phi(\mathbf{x})e^{i\omega t}\right\} \tag{1}$$

where $\Re$ is the operator that takes the real part of a complex number. The pressure in the fluid, $P(\mathbf{x}, t)$, can be computed via:

$$P(\mathbf{x}, t) = -\rho\frac{\partial\Phi}{\partial t} = \Re\left\{-i\omega\rho\phi(\mathbf{x})e^{i\omega t}\right\} \tag{2}$$

where ρ is the fluid density. This can be written in terms of a pressure RAO, $p(\mathbf{x})$, as:

$$P(\mathbf{x}, t) = \Re\left\{p(\mathbf{x})e^{i\omega t}\right\} \tag{3}$$

where

$$p(\mathbf{x}) \quad = \quad -i\omega\rho\phi(\mathbf{x}) \tag{4}$$

The velocity of the fluid, $\mathbf{V}(\mathbf{x}, t)$, is given by:

$$\mathbf{V}(\mathbf{x}, t) = \nabla\Phi = \Re\left\{\nabla\phi(\mathbf{x})\, e^{i\omega t}\right\} \tag{5}$$

In RAO terms this is:

$$\mathbf{V}(\mathbf{x}, t) = \Re\left\{\mathbf{v}(\mathbf{x})e^{i\omega t}\right\} \tag{6}$$

where

$$\mathbf{v}(\mathbf{x}) = \nabla\phi(\mathbf{x}) \tag{7}$$

For a disturbed sea state (i.e. the sea state in the vicinity of a vessel), with disturbed velocity potential $\phi_d(\mathbf{x})$, OrcaFlex defines a disturbance RAO, $\mathcal{P}(\mathbf{x})$, as:

$$\mathcal{P}(\mathbf{x}) = \frac{\phi_d(\mathbf{x})}{\phi_u(\mathbf{x})} \tag{8}$$

where $\phi_u(\mathbf{x})$ is the velocity potential RAO corresponding to the *undisturbed* sea state that would have been present in the absence of the vessel (see below for more details). The reason that we work in terms of $\mathcal{P}(\mathbf{x})$ instead of $\phi_d(\mathbf{x})$ is because $\mathcal{P}(\mathbf{x})$ is generally an RAO with unit amplitude and zero phase far away from the vessel. This makes it a lot easier to interpolate between the user data points because $\mathcal{P}(\mathbf{x})$ usually varies less rapidly with position than $\phi_d(\mathbf{x})$ does.

The gradient, $\nabla\mathcal{P}$, of the disturbance RAO can be used by OrcaFlex to compute the disturbed velocity RAO, $\mathbf{v}_d$, from the undisturbed quantities ϕ_u and $\mathbf{v}_u$:

$$\mathbf{v}_d = \nabla\phi_d = \nabla(\mathcal{P}\phi_u) = \phi_u\nabla\mathcal{P} + \mathcal{P}\nabla\phi_u = \phi_u\nabla\mathcal{P} + \mathcal{P}\mathbf{v}_u \tag{9}$$

WAMIT outputs the non-dimensional pressure RAOs, $\bar{p}(\mathbf{x})$, and velocity RAOs, $\bar{\mathbf{v}}(\mathbf{x})$, in the fluid domain (see sections 3.5 and 3.7 of the WAMIT v7.0 user manual for the formulae given in this section). A non-dimensional pressure RAO in WAMIT is equal to the non-dimensional velocity potential RAO, $\bar{\phi}$, defined via:

$$\bar{p} = \bar{\phi} = \frac{\phi}{(igA/\omega)} \tag{10}$$

where g is the acceleration due to gravity and A is the incident wave amplitude. A non-dimensional velocity RAO, $\bar{\mathbf{v}}(\mathbf{x})$, is similarly defined as:

$$\bar{\mathbf{v}}(\mathbf{x}) = \frac{\mathbf{v}(\mathbf{x})}{igA/(wL)} \tag{11}$$

where L is the length scale parameter associated with the WAMIT diffraction analysis. The various factors in these equations are chosen to ensure that:

$$\bar{\mathbf{v}} = \bar{\nabla}\bar{\phi} \tag{12}$$

where $\bar{\nabla} = L\nabla$ is the non-dimensional gradient operator. WAMIT outputs pressure, $\bar{p}_d$, and velocity, $\bar{\mathbf{v}}_d$, RAOs for the disturbed sea. Equation (2.1) in the WAMIT theory manual gives the velocity potential RAO, ϕ_u, for the undisturbed case:

$$\phi_u = \frac{igA}{\omega} Z(kz) e^{-ik(x\cos\beta + y\sin\beta)} \tag{13}$$

where k is the wavenumber and $Z(kz)$ controls the behaviour of the velocity potential with depth (the exponential decay factor). Computing the gradient of this expression gives the undisturbed fluid velocity RAO, $\mathbf{v}_u$.

When OrcaFlex imports sea state disturbance RAOs from a WAMIT *.out* file it reads the sections entitled *Hydrodynamic Pressure In The Fluid Domain* and *Velocity Vector In The Fluid Domain*. The WAMIT pressure RAO results give $\bar{p}_d$, which permits $\bar{\phi}_d$, and hence ϕ_d, to be calculated; the WAMIT velocity vector results give $\bar{\mathbf{v}}_d$, from which $\bar{\nabla}\bar{\phi}_d$ and $\nabla\phi_d$ can be computed. OrcaFlex then calculates the sea state disturbance RAO, $\mathcal{P}$, and its gradient, $\nabla\mathcal{P}$, using the following equations:

$$\boxed{\mathcal{P} = \frac{\phi_d}{\phi_u} \qquad \nabla\mathcal{P} = \frac{\mathbf{v}_d - \mathcal{P}\mathbf{v}_u}{\phi_u}} \tag{14}$$

where the latter equation is derived as follows:

$$\begin{aligned}
\nabla\mathcal{P} &= \nabla\left(\frac{\phi_d}{\phi_u}\right) && (15)\\
&= \frac{\phi_u\nabla\phi_d - \phi_d\nabla\phi_u}{\phi_u^2} && (16)\\
&= \frac{\phi_u\nabla\phi_d - \mathcal{P}\phi_u\nabla\phi_u}{\phi_u^2} && (17)\\
&= \frac{\nabla\phi_d - \mathcal{P}\nabla\phi_u}{\phi_u} && (18)\\
&= \frac{\mathbf{v}_d - \mathcal{P}\mathbf{v}_u}{\phi_u} && (19)
\end{aligned}$$

Care needs to be taken when using these equations to ensure that any appropriate conventions (e.g. phase leads/lags) are accounted for.

Appendix B

Matlab codes

B.1 Generates a specter when from time realizations

```
function [specfreq, specter] = Spectergen(H)

n=length(H(1,:));

dt = (H(1,n)-H(1,1))/(n-1);

win = [850 11600]-850;
win = round(win/dt +1);

t = H(1,win(1):win(2));
elev = H(2,win(1):win(2));
melev = mean(elev);

fs = 1/dt;
window = round(length(t)/60);
noverlap = 10;

[specter, specfreq] = pwelch(elev-melev,window,noverlap,[],fs);
end
```

B.2 Generates a realization of vertical motions in a given point based on heave, roll and pitch

```
function H = Heave(acqu, locn, moonpoolType, plotOrNot)
%% Input treatment
if moonpoolType == 1
    COG = [71.1 0 10];
    acqu = strcat('/Volumes/My Book/C3 - ...
        Vessel/Results/Wave tests/standard moonpool/',acqu);
elseif moonpoolType == 2
    COG = [70.2 0 10.5];
    acqu = strcat('/Volumes/My Book/C3 - ...
        Vessel/Results/Wave tests/enlarged moonpool/',acqu);
else
    disp('Please enter moonpool type correctly while ...
        calling the Heave function. 1 = standard, 2 = ...
        enlarged.');
end

%% Heave motion ship

DataPath = strcat(acqu,'.a13/test_003.dat');

fid = fopen(DataPath,'r');
nu3 = fscanf(fid,'%f %f',[2,inf]);
fclose(fid);

%% Roll motion ship

DataPath = strcat(acqu,'.a13/test_004.dat');

fid = fopen(DataPath,'r');
nu4 = fscanf(fid,'%f %f',[2,inf]);
fclose(fid);


%% Pitch motion ship

DataPath = strcat(acqu,'.a13/test_005.dat');

fid = fopen(DataPath,'r');
nu5 = fscanf(fid,'%f %f',[2,inf]);
fclose(fid);


%% Heave at location

delX = locn - COG;

H(1,:) = nu3(1,:);
```

```
44  H(2,:) = nu3(2,:) - delX(2)*sin(nu4(2,:)*pi/180) - ...
        delX(1)*sin(nu5(2,:)*pi/180);
45
46  %% Plotting
47  if plotOrNot == 1
48
49      %line_width = 1.5;
50      font_size  = 18;
51      mkr_size   = 8;
52      %set(0, 'DefaultLineLineWidth' , line_width);
53      set(0, 'DefaultAxesFontSize' , font_size);
54      set(0, 'DefaultLineMarkerSize' , mkr_size);
55
56      plot(H(1,:),H(2,:)),grid
57      xlabel('Time, [s]')
58      ylabel('Vertical motion, [m]')
59      title(['Vertical motion at X = ', num2str(locn(1)),', Y ...
            = ', num2str(locn(2)), ', Z = ',num2str(locn(3))])
60  end
61
62  end
```

B.3 Generates all the presented spectra for each module elevation

```
function  ModTestAnal()

close all
load('input.mat');

S1loc = [84.1 0 6.5];

m = zeros(4,length(Tp));
mL = zeros(4,length(Tp));

if MPoolType == 1
    mpt = 'standard';
elseif MPoolType == 2
    mpt = 'enlarged';
else
    disp('Wrong mooonpool type!');
    return

end
disp(' ');
disp(['Analysis started for ', Elevation,'. Moonpool type ...
    ', mpt])

for i=1:length(Tp)
    disp(' ');
    disp(['Run ',num2str(i), ' started']);
    vm = Heave(char(acqu(i)),S1loc,MPoolType,0);
    disp('    Vertical motions analysis completed!');

    DataPath = strcat('/Volumes/My Book/C3 - ...
        Vessel/Results/Wave tests/',mpt,' ...
        moonpool/',char(acqu(i)),'.a13/Asgard_Loads_007.dat');

    fid = fopen(DataPath,'r');
    Load = fscanf(fid,'%f %f',[2,inf]);
    fclose(fid);

    DataPath = strcat('/Volumes/My Book/C3 - ...
        Vessel/Results/Wave tests/',mpt,' ...
        moonpool/',char(acqu(i)),'.a13/test_014.dat');

    fid = fopen(DataPath,'r');
    S1 = fscanf(fid,'%f %f',[2,inf]);
    fclose(fid);

    DataPath = strcat('/Volumes/My Book/C3 - ...
        Vessel/Results/Wave tests/',mpt,' ...
        moonpool/',char(acqu(i)),'.a13/test_043.dat');
```

```
42
43      fid = fopen(DataPath,'r');
44
45      if fid<0
46          DataPath = strcat('/Volumes/My Book/C3 - ...
                Vessel/Results/Wave tests/',mpt,' ...
                moonpool/',char(acqu(i)),'.a13/test_036.dat');
47          fid = fopen(DataPath,'r');
48      end
49
50      if fid<0
51          disp(['Acquisition error @ ', DataPath])
52          return
53      end
54
55      OceE = fscanf(fid,'%f %f',[2,inf]);
56      fclose(fid);
57
58      DataPath = strcat('/Volumes/My Book/C3 - ...
            Vessel/Results/Wave tests/',mpt,' ...
            moonpool/',char(acqu(i)),'.a13/Asgard_Loads_021.dat');
59
60      fid = fopen(DataPath,'r');
61      OceL = fscanf(fid,'%f %f',[2,inf]);
62      fclose(fid);
63
64      disp('    Force and elevation read off completed!');
65
66      [specfreqvm, spectervm] = Spectergen(vm);
67      [specfreqS1, specterS1] = Spectergen(S1);
68      [specfreqL, specterL] = Spectergen(Load);
69
70      Svm=torsethaugen(specfreqvm*2*pi,[4.5 Tp(i)],0);
71      SS1=torsethaugen(specfreqS1*2*pi,[4.5 Tp(i)],0);
72      SL=torsethaugen(specfreqL*2*pi,[4.5 Tp(i)],0);
73
74      RAOvm = sqrt(spectervm./(Svm.S*2*pi));
75      RAOS1 = sqrt(specterS1./(SS1.S*2*pi));
76      RAOL = sqrt(specterL./(SL.S*2*pi));
77
78
79      figure('Name','Spectra related to surface elevation ...
            inside moonpool','NumberTitle','off');
80      plot(SS1.w/(2*pi),SS1.S*2*pi, 'b',specfreqvm, ...
            spectervm, 'r',specfreqS1, specterS1, 'k')
81      legend('Ocean waves', 'Vertical vessel motions', ...
            'Surface elevation')
82      xlabel('Frequency, [1/s]')
83      ylabel('Spectral density, [m^2s]')
84      grid on;
85      set(gca,'GridLineStyle','-');
86      if Tp(i) == 8
87          axis([0 0.5 0 20])
88      elseif Tp(i) == 9
```

```
89          axis([0 0.5 0 25])
90      elseif Tp(i) == 11
91          axis([0 0.5 0 25])
92      else
93          axis([0 0.5 0 40])
94      end
95      title([Elevation,' elevation spectra Tp = ...
            ',num2str(Tp(i))])
96      saveas(gcf,['Elevation ',Elevation,', Tp = ...
            ',num2str(Tp(i)),', run ',num2str(i)], 'pdf')
97
98
99      figure('Name','RAO between surface elevation inside ...
            moonpool and irregular waves','NumberTitle','off');
100     plot(SS1.w/(2*pi), RAOS1, OceE(1,:), OceE(2,:))
101     legend('Student Analysis', 'Oceanide analysis')
102     xlabel('Frequency, [1/s]')
103     ylabel('RAO, [m/m]')
104     grid on;
105     set(gca,'GridLineStyle','-');
106     axis([0.05 0.3 0 1.5])
107     title([Elevation, ' RAO Tp = ',num2str(Tp(i))])
108     saveas(gcf,['RAO ', Elevation,', Tp = ...
            ',num2str(Tp(i)),', run ',num2str(i)], 'pdf')
109
110     df = specfreqS1(2)-specfreqS1(1);
111
112     for j = 1:length(specfreqS1)
113         m(1,i) = m(1,i)+specterS1(j)*df;
114         m(2,i) = m(2,i)+specterS1(j)*df*specfreqS1(j);
115         m(3,i) = m(3,i)+specterS1(j)*df*specfreqS1(j)^2;
116         m(4,i) = m(4,i)+specterS1(j)*df*specfreqS1(j)^3;
117     end
118
119
120     figure('Name','Spectrum of vertical force on ...
            module','NumberTitle','off');
121     plot(specfreqL, specterL)
122
123     xlabel('Frequency, [1/s]')
124     ylabel('Spectral density, [kN^2s]')
125     grid on;
126     set(gca,'GridLineStyle','-');
127     axis([0 0.3 0 max(specterL)*1.05])
128     title([Elevation, ' Force spectrum Tp = ',num2str(Tp(i))])
129     saveas(gcf,['Force ',Elevation,', Tp = ...
            ',num2str(Tp(i)),', run ',num2str(i)], 'pdf')
130
131     figure('Name','RAO of vertical force on ...
            module','NumberTitle','off');
132     plot(SL.w/(2*pi), RAOL, OceL(1,:), OceL(2,:))
133     legend('Student Analysis', 'Oceanide Analysis')
134     xlabel('Frequency, [1/s]')
135     ylabel('Transfer function, [kN/m]')
```

```
136      grid on;
137      set(gca,'GridLineStyle','-');
138      axis([0.05 0.3 0 max(OceL(2,:))*1.2])
139      title([Elevation, ' Transfer function Tp = ...
             ',num2str(Tp(i))])
140      saveas(gcf,['Force RAO ',Elevation,', Tp = ...
             ',num2str(Tp(i)),', run ',num2str(i)], 'pdf')
141
142      dfL = specfreqL(2)-specfreqL(1);
143
144      for j = 1:length(specfreqL)
145          mL(1,i) = mL(1,i)+specterL(j)*dfL;
146          mL(2,i) = mL(2,i)+specterL(j)*dfL*specfreqL(j);
147          mL(3,i) = mL(3,i)+specterL(j)*dfL*specfreqL(j)^2;
148          mL(4,i) = mL(4,i)+specterL(j)*dfL*specfreqL(j)^3;
149      end
150
151      vmRAO(i,:) = RAOvm;
152
153      WaveRAO(i,:) = RAOS1;
154
155      ForceRAO(i,:) = RAOL;
156  end
157  ForceRAOf = SL.w/(2*pi);
158  WaveRAOf = SS1.w/(2*pi);
159  vmRAOf = Svm.w/(2*pi);
160
161  figure('Name','RAO of vertical force on ...
         module','NumberTitle','off');
162  plot(ForceRAOf,ForceRAO(1,:),ForceRAOf,ForceRAO(2,:),ForceRAOf,ForceRAO(3,:),ForceRAOf,For
163  legend(strcat('Tp ',num2str(Tp(1))),strcat('Tp ...
         ',num2str(Tp(2))),strcat('Tp ...
         ',num2str(Tp(3))),strcat('Tp ...
         ',num2str(Tp(4))),strcat('Tp ...
         ',num2str(Tp(5))),strcat('Tp ',num2str(Tp(6))));
164  xlabel('Frequency, [1/s]')
165  ylabel('Transfer function, [kN/m]')
166  grid on;
167  set(gca,'GridLineStyle','-');
168  axis([0.05 0.3 0 max(OceL(2,:))*1.2])
169  title([Elevation, ' Transfer function'])
170  saveas(gcf,['Force RAO ',Elevation], 'pdf')
171
172  figure('Name','RAO between surface elevation inside ...
         moonpool and irregular waves','NumberTitle','off');
173  plot(WaveRAOf,WaveRAO(1,:),WaveRAOf,WaveRAO(2,:),WaveRAOf,WaveRAO(3,:),WaveRAOf,WaveRAO(4,
174  legend(strcat('Tp ',num2str(Tp(1))),strcat('Tp ...
         ',num2str(Tp(2))),strcat('Tp ...
         ',num2str(Tp(3))),strcat('Tp ...
         ',num2str(Tp(4))),strcat('Tp ...
         ',num2str(Tp(5))),strcat('Tp ',num2str(Tp(6))))
175  xlabel('Frequency, [1/s]')
176  ylabel('RAO, [m/m]')
177  grid on;
```

```
178 set(gca,'GridLineStyle','-');
179 axis([0.05 0.3 0 1.5])
180 title([Elevation, ' Transfer function of surface elevation'])
181 saveas(gcf,['RAO ', Elevation], 'pdf')
182
183 figure('Name','RAO heave','NumberTitle','off');
184 plot(vmRAOf,vmRAO(1,:),vmRAOf,vmRAO(2,:),vmRAOf,vmRAO(3,:),vmRAOf,vmRAO(4,:),vmRA
185 legend(strcat('Tp ',num2str(Tp(1))),strcat('Tp ...
        ',num2str(Tp(2))),strcat('Tp ...
        ',num2str(Tp(3))),strcat('Tp ...
        ',num2str(Tp(4))),strcat('Tp ...
        ',num2str(Tp(5))),strcat('Tp ',num2str(Tp(6))))
186 xlabel('Frequency, [1/s]')
187 ylabel('RAO, [m/m]')
188 grid on;
189 set(gca,'GridLineStyle','-');
190 axis([0 0.3 0 2.5])
191 title([Elevation, ' Transfer function heave'])
192 saveas(gcf,['RAO heave', Elevation], 'pdf')
193
194 for i = 1: length(vmRAOf)
195
196     if vmRAOf(i)<0.05
197         MRAOvm(i) = 0;
198     else
199         MRAOvm(i) = mean(vmRAO(:,i));
200     end
201 end
202 figure('Name','Mean RAO heave','NumberTitle','off');
203 plot(vmRAOf,MRAOvm)
204 xlabel('Frequency, [1/s]')
205 ylabel('RAO, [m/m]')
206 grid on;
207 set(gca,'GridLineStyle','-');
208 axis([0 0.3 0 2.5])
209 title([Elevation, ' Mean Transfer function heave'])
210 saveas(gcf,['Mean RAO heave', Elevation], 'pdf')
211
212 Hm0 = 4 * sqrt(m(1,:));
213 Tm02 = sqrt(m(1,:)./m(3,:));
214
215 Fm0 = 4 * sqrt(mL(1,:));
216 TmL02 = sqrt(mL(1,:)./mL(3,:));
217
218 save('Responsestatistics.mat','m','Hm0','Tm02','mL', ...
        'Fm0','TmL02','WaveRAO','ForceRAO','vmRAO','MRAOvm','WaveRAOf','ForceRAOf','vm
219
220 disp(' ');
221 disp('Analysis completed!');
222 end
```

B.4 Gathers finished results for each module elevation and puts it together

```
function FinalAnal()
close all
elev = {'M1' 'M2' 'M3' 'M4'};

force = zeros(length(elev),6);
surface = zeros(length(elev),6);
Tpm = zeros(length(elev),6);

for i = 1:length(elev)
    DataPath = strcat(char(elev(i)),'/Responsestatistics.mat');
    load(DataPath);

    DataPath = strcat(char(elev(i)),'/input.mat');
    load(DataPath);

    Tpm(i,:) = Tp;
    force(i,:) = Fm0/2;
    surface(i,:) = Hm0;

end

figure('Name','Significant Force','NumberTitle','off');
plot(Tpm(1,:),force(1,:),'+',Tpm(2,:),force(2,:),'+',Tpm(3,:),force(3,:),'+',Tpm(4,:),forc
    'MarkerSize',10);
legend('M1','M2','M3','M4');
axis([7 15 min(force(:,4))*0.95 max(force(:,2))*1.05]);
xlabel('Peak frequency, Tp [1/s]')
ylabel('Load [kN]')
title('Significant load amplitude')
saveas(gcf,'Significant load amplitude', 'pdf')

figure('Name','Significant Wave','NumberTitle','off');
plot(Tpm(1,:),surface(1,:),'+',Tpm(2,:),surface(2,:),'+',Tpm(3,:),surface(3,:),'+',Tpm(4,:
    'MarkerSize',10);
legend('M1','M2','M3','M4');
axis([7 15 2 3]);
xlabel('Peak frequency, Tp [1/s]')
ylabel('Wave height [m]')
title('Significant wave height inside moonpool')
saveas(gcf,'Significant wave height inside moonpool', 'pdf')

end
```

Appendix C

Module dimensions

Reference volume:		94.2	m^3
Displacement:		96.6	te
Inertia:	Ixx	6 216.7	te.m²
	Iyy	8 518.8	te.m²
	Izz	5 899.0	te.m²
Main dimensions:	X	14.2	m
	Y	10.4	m
	Z	6.3	m

Figure C.1: Module dimensions of inlet-cooler

Reference volume:		84.7 m^3
Displacement:		86.8 te
Inertia:	Ixx	11 269.8 te.m²
	Iyy	12 078.1 te.m²
	Izz	4 072.6 te.m²
Main dimensions:	X	11.3 m
	Y	7.7 m
	Z	9.7 m

Figure C.2: Module dimensions of compressor

Reference volume:		11.4 m^3
Displacement:		11.7 te
Inertia:	Ixx	352.8 te.m²
	Iyy	369.5 te.m²
	Izz	95.6 te.m²
Main dimensions:	X	4.71 m
	Y	3.09 m
	Z	6.67 m

Figure C.3: Module dimensions of pump